

**KERNFORSCHUNGSZENTRUM  
KARLSRUHE**

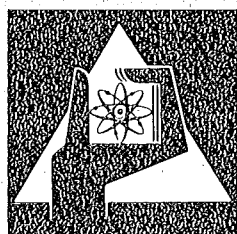
Juni 1975

KFK 2166

Institut für Neutronenphysik und Reaktortechnik  
Projekt Schneller Brüter

**Transient Hydraulics and Heat Transfer  
in a Turbulent Flow**

H. Kawamura



**GESELLSCHAFT  
FÜR  
KERNFORSCHUNG M.B.H.**

**KARLSRUHE**

Als Manuskript vervielfältigt

Für diesen Bericht behalten wir uns alle Rechte vor

GESELLSCHAFT FÜR KERNFORSCHUNG M. B. H.  
KARLSRUHE

KERNFORSCHUNGSZENTRUM KARLSRUHE

KFK 2166

Institut für Neutronenphysik und Reaktortechnik  
Projekt Schneller Brüter

Transient Hydraulics and Heat Transfer  
in a Turbulent Flow

H. Kawamura\*

Gesellschaft für Kernforschung mbH., Karlsruhe

---

\* Delegated from Japan Atomic Energy Research Institute, Tokai,  
Ibaraki, 319-11, Japan



## Abstract

In a reactor transient analysis, the friction factor and the heat transfer coefficient are assumed equal to the steady state values even in a transient state. This quasi-static assumption has been examined in the present paper.

The transient turbulent flow in a circular tube subjected to a step change of pressure drop was calculated numerically. Transient variations of the friction factor and the heat transfer coefficient were obtained. Effects of the Reynolds number and a wall heat capacity were studied.

The quasi-static momentum equation was found to be approximately valid for both accelerated and decelerated turbulent flow. The quasi-static energy equation was also valid for the transients of gas cooled reactors.

## Zusammenfassung

### Instationäre Hydrodynamik und instationärer Wärmeübergang in turbulenten Strömungen

In instationären Analysen von Kernreaktoren wird angenommen, daß die Widerstandsbeiwerte und die Wärmeübergangszahlen für den stationären und instationären Zustand gleich sind. Diese quasistationäre Näherung wird im vorliegenden Bericht untersucht.

Die instationäre turbulente Strömung in einem runden Rohr wurde numerisch berechnet. Der Druckabfall wurde stufenweise geändert. Die instationäre Veränderung des Widerstandsbeiwertes und der Wärmeübergangszahl wurde bestimmt, und der Einfluß von Reynoldszahl und Wandwärmekapazität wurde untersucht. Es konnte gezeigt werden, daß die quasistationäre Impulsgleichung gültig ist für beschleunigte und verzögerte turbulente Strömungen. Die quasistationäre Energiegleichung ist auch gültig für gasgekühlte Kernreaktoren.

## Contents

Abstract	Page
1. Introduction	1
2. Numerical Analysis	2
2.1 Assumptions	2
2.2 Two-dimensional equations	3
2.3 Numerical calculation	7
2.4 Quasi-static calculation	8
2.5 Steady state calculation	9
3. Transient Hydraulics	9
3.1 Variation of velocity	9
3.2 Time for the flow to reach the steady state	10
3.3 Variation of $f/f_{st}$	11
3.4 Comparison with the quasi-static calculation	12
4. Transient Heat Transfer	13
4.1 Variation of heat transfer coefficient	13
4.2 Case of deceleration	14
4.3 Case of acceleration	15
4.4 Liquid metal cooling	18
5. Application to Reactors	19
6. Conclusions	20
Acknowledgements	21
Nomenclature	22
References	24
Appendix A	25
Tables	28
Figures	30

## 1. Introduction

In a reactor transient analysis, the momentum equation and the energy equation for a coolant flow must be solved. The friction factor and the heat transfer coefficient are introduced into these equations, but these are always assumed equal to the steady state values even in a transient state. This assumption is made in almost all the safety analysis codes, but has not been examined well. The purpose of the present paper is to examine the validity of the quasi-static assumption by analyzing the transient turbulent hydraulics and heat transfer.

The momentum equation solved in the reactor transient analysis is

$$\frac{\partial \bar{u}}{\partial t} = \frac{g_c}{\rho_f} \left| \frac{\partial P}{\partial x} \right| - f \frac{\bar{u}^2}{D/2}, \quad (1)$$

where  $f$  is the friction factor defined as

$$f = \tau / \frac{1}{2} \rho_f \bar{u}^2. \quad (2)$$

The energy equation is

$$\frac{\partial \bar{T}_f}{\partial t} + \bar{u} \frac{\partial \bar{T}_f}{\partial x} = \alpha \frac{4}{D(\rho c_p)_f} (T_w - \bar{T}_f), \quad (3)$$

where  $\alpha$  is the heat transfer coefficient defined as

$$\alpha = q_n / (T_w - \bar{T}_f). \quad (4)$$

By introducing  $f$  and  $\alpha$ , one need not solve transient profiles of the velocity or temperature. These equations are suited for a large safety analysis code. However, as the transient values of  $f$  and  $\alpha$  are not known, the steady state values are always used in the transient state also. So, these equations are called quasi-static equations.

Many works have been made for the transient laminar heat transfer, but relatively few works for the transient turbulent heat transfer. Sparrow-Siegel<sup>(1)</sup> solved the transient energy equation for stepwise time variation of wall temperature. Soliman<sup>(2)</sup> studied the transient heat transfer from a plate of a finite heat capacity to a developing flow of water. The present author<sup>(3)</sup> analyzed the transient turbulent heat transfer in an annulus. The flow was steady and the heat input was increased stepwisely. The conditions for the quasi-static assumption were studied.

In the present paper, the transient two-dimensional momentum and energy equations are formulated and solved for the step change of the pressure drop with a constant heat input. These solutions are compared with those of the quasi-static equations. Effects of the Reynolds number and the wall heat capacity are studied, and the validity of the quasi-static equation is examined.

This work was done in the course of the development of a transient analysis code for Gas Cooled Fast Reactor (GCFR). So, the primary interest lies in GCFR, but attentions are paid also for other types of reactors such as PWR and LMFBR.

## 2. Numerical Analysis

### 2.1 Assumptions

- 1) A very long circular tube is assumed, so the flow is fully developed.
- 2) The heating wall has a finite thermal capacity, but the temperature distribution inside the wall is neglected.
- 3) The outer surface of the wall is insulated.
- 4) Properties are independent of the temperature.
- 5) The Prandtl's mixing length theory is applicable.

## 2.2 Two-dimensional equations

A co-ordinate is shown in Fig. 1. A wall is heated from  $x = 0$ . The momentum equation is

$$\frac{\partial u}{\partial t} = \frac{\xi_c}{\rho_f} \left| \frac{\partial P}{\partial x} \right| + \frac{1}{r} \frac{\partial}{\partial r} \left[ (\epsilon_M + \nu) r \frac{\partial u}{\partial r} \right]. \quad (5)$$

The energy equation is

$$\frac{\partial T}{\partial t} + u \frac{\partial T}{\partial x} = \frac{1}{r} \frac{\partial}{\partial r} \left[ (\epsilon_H + a_f) r \frac{\partial T}{\partial r} \right]. \quad (6)$$

These both equations contain two co-ordinates  $x$  and  $r$ , but Eq. (5) is one-dimensional because  $u$  does not vary in the direction of  $x$ . However, Eq. (5) will be called also as two-dimensional for convenience.

Boundary conditions are

$$r = D/2, \text{ (at the wall)}$$

$$u(r_w, t) = 0 \quad (7)$$

$$T(x, r_w, t) = T_w(x, t) \quad (8)$$

$$q_n(x, t) = - \lambda_f \frac{\partial T}{\partial r} \Big|_{r=r_w}. \quad (9)$$

The heat balance in the wall is

$$q_n(x, t) = q_G - H \frac{\partial}{\partial t} T_w(x, t), \quad (10)$$

where  $q_G$  is the heat generation rate in the wall and independent of time. Other conditions are

$$r = 0, \text{ (at the center)}$$

$$\frac{\partial u}{\partial r} = 0 \quad (11)$$

$$\frac{\partial T}{\partial r} = 0 \quad (12)$$

$x = 0$ , (at entrance)

$$T(0, r, t) = T_{in} \equiv 0 \quad (13)$$

The pressure drop changes stepwisely as follows:

$$\left| \frac{\partial P}{\partial x} \right| = \begin{cases} P_{x,0} & t \leq 0 \\ P_{x,1} & t > 0. \end{cases} \quad (14)$$

Initial steady state profiles of  $u$  and  $T$  for  $P_{x,0}$  were calculated at first, then the transient calculation was made.

The momentum eddy diffusivity  $\epsilon_M$  in the steady state has been studied intensively; however,  $\epsilon_M$  in the transient state is not known yet. Some sophisticated turbulence models are proposed, but many of them are so complicated that even the calculation of a steady flow needs a very long time. Some turbulence models can calculate a transient flow, but those are still not suited for calculating the transient heat transfer at the same time. Here, a simple turbulence model, Prandtl's mixing length theory, is adopted to calculate the momentum eddy diffusivity.

The momentum eddy diffusivity is calculated by

$$\epsilon_M = \ell^2 \left| \frac{\partial u}{\partial r} \right|. \quad (15)$$

Here,  $\ell$  is the Prandtl's mixing length, calculated by the following method of Patankar and Spalding<sup>(4)</sup>.

In the central region of a tube,  $\ell$  is usually taken as uniform. It is nearly 8 - 10 % of the boundary layer thickness; that is, 4-5 % of the tube diameter.

$$\ell_c = \lambda_\ell D \quad (16)$$

In the present calculation  $\lambda_\ell$  is 0.045.

Near the wall,  $\ell$  is proportional to the distance from the wall,  $y$ . The proportionality constant is 0.36 - 0.4. Very close to the wall,  $\ell$  is damped as postulated by van Driest<sup>(5)</sup>:

$$\ell_w = \kappa_\ell y [1 - \exp(-y^+/A^+)] \quad (17)$$

where  $A^+$  is a damping constant and  $y^+$  is  $yu^*/\nu$ .

The constant  $A^+$  is about 20 - 30 depending on the Reynolds number.

Figure 2 illustrates  $\ell_c$  and  $\ell_w$ . To avoid a broken point at the intersection of  $\ell_c$  and  $\ell_w$ , the following equation is used for  $\ell$  finally.

$$\frac{1}{\ell^2} = \frac{1}{\ell_c^2} + \frac{1}{\ell_w^2} \quad (18)$$

This equation (18) gives  $\epsilon_M$  with Eq. (15). However,  $\epsilon_M$  becomes zero where  $\partial u/\partial r = 0$ ; i.e; at the center of the tube. To avoid this defect, the following assumption is made:

$$\ell \left| \frac{\partial u}{\partial y} \right| = \lambda_u u, \text{ if } \ell \left| \frac{\partial u}{\partial y} \right| \leq \lambda_u u, \quad (19)$$

where  $u$  is a local velocity and  $\lambda_u$  is a constant equal to 0.01. The condition of Eq. (19) is satisfied at only a few meshes near the center.

The thermal eddy diffusivity is obtained from the eddy diffusivity ratio  $\sigma = \epsilon_H/\epsilon_M$ . Mizushima<sup>(5)</sup> proposed a correlation of  $\sigma$  as follows:

$$\sigma = 1.5 \phi [1 - \exp(-1/\phi)] \quad (20)$$

$$\phi = \frac{(\epsilon_M/\nu) \text{Pr}}{4.13 + 0.743 (\epsilon_M/\nu)^{1/2} \text{Pr}^{1/3}} \quad (21)$$

These methods are widely accepted for the calculation of the steady state turbulent flow. Here, it is assumed that these are applicable also for the transient flow. The momentum eddy diffusivity represents the momentum exchange between turbulent eddies. The scale of the eddies are so small that the time scale of the momentum exchange is smaller than the time scale of the whole transient. So, the steady state mixing length theory is assumed in the transient state also.

The order of time for the momentum exchange between eddies is roughly

$$t_{\text{eddy}} \sim \frac{l^2}{\epsilon_M} \quad (22)$$

The order of time for the flow to reach the steady state will be obtained in the latter section of the present paper as follows:

$$t_{\text{flow}} \sim \frac{1}{f \cdot \text{Re}} \frac{D^2}{\nu} \quad (23)$$

The ratio of these two time scales is

$$\frac{t_{\text{eddy}}}{t_{\text{flow}}} \sim f \cdot \text{Re} \cdot \left(\frac{l}{D}\right)^2 \frac{\nu}{\epsilon_M} \quad (24)$$

At  $\text{Re} = 10^5$ , for example,  $f$  is  $4.5 \times 10^3$ ,  $(\epsilon_M/\nu) \sim 100$  and  $l/D \sim 0.045$ . So, the ratio becomes  $t_{\text{eddy}}/t_{\text{flow}} \sim 10^2$ .

This ratio does not depend much on the Reynolds number.

Although the steady state mixing theory is used for  $\epsilon_M$ , the value of  $\epsilon_M$  is not equal to its steady state value. The momentum equation Eq. (5) gives a transient velocity profile, and then Eq. (15) gives a transient  $\epsilon_M$ .

### 2.3 Numerical calculation

The equations in the preceding section were transformed into non-dimensional forms, and then finite difference formulae were obtained. The non-dimensional forms are listed in Appendix A. It can be shown that the whole solution is determined by the following non-dimensional variables and their combinations.

Initial and final Reynold number,  $Re_0, Re_1$   
Prandtl number,  $Pr$ ,  
Heating length,  $x/D$   
Heat capacity ratio,  $\hat{H} = \frac{(\rho c_p)_w d_w}{(\rho c_p)_f D} (1 + d_w/D)$  (25)

The numerical calculation is made by the implicit method. The solution is always stable irrespective of the time mesh.

The biggest difficulty in the numerical calculation is that the thickness of the laminar sublayer near the wall tends to be very small compared with the tube diameter. The laminar sublayer is the layer where the velocity increases nearly linearly. This thickness is about  $10^{-4}$  of the tube diameter at  $Re = 10^6$ .

The radial mesh size adjacent to the wall must be less than this thickness, so the total radial mesh number becomes more than  $10^4$ . The steady state may be calculated with this mesh number, but not the transient state.

In the present study, the radial mesh is given in geometrical progression as follows.

$$\Delta r_k = a \Delta r_{k+1}, \quad (26)$$

where  $\Delta r_k = r_k - r_{k-1}$  and

$$r_M = D/2, r_1 = 0 \quad (27)$$

$$r_M - r_{M-1} = h (v/u^*)$$

The mesh size  $\Delta r_k$  is limited up to 0.020 D to avoid large mesh in the tube center. The values used for a and h are 1.2 - 1.3 and 1-3 respectively. The total mesh number can be reduced down to less than 70 even at  $Re = 10^6$ .

The diffusion term in Eqs. (5) and (6) has the common form:

$$\frac{1}{r} \frac{\partial}{\partial r} \left[ E r \frac{\partial \phi}{\partial r} \right], \quad (28)$$

where E denotes either  $E = \epsilon_M + v$  or  $E = \epsilon_M + \alpha$ . In the present analysis, the diffusion coefficient E and the radial mesh size are both a function of r. A new difference formula of Eq. (28) has been derived as shown in Table 1.

#### 2.4 Quasi-static calculation

The quasi-static equations are

$$\frac{d\bar{u}}{dt} = \frac{g_c}{\rho_f} \left| \frac{\partial P}{\partial x} \right| - f_{st} \frac{\bar{u}^2}{D/2} \quad (29)$$

$$\frac{\partial \bar{T}_f}{\partial t} + \bar{u} \frac{\partial \bar{T}_f}{\partial x} = \alpha_{st} \frac{4}{D(\rho c_p)_f} (T_w - \bar{T}_f) \quad (30)$$

$$\alpha_{st} (T_w - \bar{T}_f) = q_G - H \frac{\partial}{\partial t} T_w(x,t) \quad (31)$$

$$x = 0: \bar{T}_f = T_{in} \equiv 0 \quad (32)$$

The steady state friction factor  $f_{st}$  and heat transfer coefficient  $\alpha_{st}$  are obtained from the numerical calculation of Eqs. (5), (6). These quasi-static equations are also transformed into finite difference formulae and solved numerically.

## 2.5 Steady state calculation

The steady state was calculated at first to test the validity of the present calculational method. Figure 3 shows the velocity distribution in the steady state. A solid line is the universal velocity profile. The present numerical results coincide well with the solid line.

Figure 4 illustrates the heat transfer coefficient and the friction factor in the steady state. Solid lines are the steady state correlations accepted usually. The numerical values of the heat transfer coefficient are given for  $Pr = 7, 1, 0.7$ . The friction factor does not depend on  $Pr$ . The numerical values agree fairly well with the steady state correlations.

## 3. Transient Hydraulics

### 3.1 Variation of velocity

Figure 5 illustrates an example of the transient numerical calculation. The pressure drop increases stepwisely at  $t = 0$ . The flow is accelerated from  $Re = 10^4$  to  $10^5$ . The velocity reaches a new steady state at about 1 sec in this example. The time in the abscissa is given for a water flow in a tube with  $D = 2$  cm. The other abscissa  $Z$  is a non-dimensional time which will be explained later. The suffix 1 represents the final steady state, while  $st$  represents the steady state value for the instantaneous Reynolds number.

The friction factor ratio  $f/f_{st}$  increases temporarily, and then decreases asymptotically down to 1. The peak value is about 1.7 in this example. The friction factor becomes much larger than the quasi-static value in case of the acceleration.

Figure 6 illustrates a case of deceleration from  $Re = 10^5$  to  $10^4$ . The flow reaches a new steady state at about 4 sec. The friction factor ratio  $f/f_{st}$  is slightly less than 1. The friction factor is nearly equal to the quasi-static value in case of the deceleration.

### 3.2 Time for the flow to reach the steady state

The time required for the flow to attain a steady state will be examined here. Since the approach to steady state is an asymptotic process, it is enough to know only an order of the time.

Let  $\bar{u} = \bar{u}_1 + \Delta\bar{u}$ , then Eq. (1) can be written as:

$$\frac{\partial}{\partial t} (\bar{u}_1 + \Delta\bar{u}) = 2 \frac{f_1}{D} \bar{u}_1^2 - 2 \frac{f}{D} (\bar{u}_1 + \Delta\bar{u})^2 \quad (33)$$

When the velocity  $\bar{u}$  has reached nearly the new steady state value  $\bar{u}_1$ , one can assume that  $\bar{u}_1 \gg \Delta\bar{u}$  and  $f \sim f_1$ . Then, Eq. (33) becomes

$$\frac{\partial}{\partial t} \Delta\bar{u} = - 4 \frac{f_1}{D} \bar{u}_1 \Delta\bar{u}. \quad (34)$$

Boundary conditions for  $\Delta\bar{u}$  are

$$\begin{aligned} \Delta\bar{u} &= 0 & t &\rightarrow \infty \\ \Delta\bar{u} &= \bar{u}_0 - \bar{u}_1 & t &= 0 \end{aligned} \quad (35)$$

then the solution of Eq. (34) is

$$\Delta\bar{u} = (\bar{u}_0 - \bar{u}_1) \exp \left( - 4 \frac{f_1}{D} \bar{u}_1 t \right). \quad (36)$$

This equation is valid only when  $t$  is large. Since  $e^{-3} \sim 0.05$  and  $e^{-4} \sim 0.02$ , one can find that the velocity reaches the steady state nearly at

$$t_{st,u} \sim (3-4) \cdot \frac{1}{4f_1} \frac{D}{\bar{u}_1}. \quad (37)$$

By substituting  $Re_1 = \bar{u}_1 D/\nu$ , one obtains

$$t_{st,u} \sim \frac{1}{f_1 Re_1} \cdot \frac{D^2}{\nu} \quad (38)$$

This is the same equation as Eq. (23) used in the preceding chapter.

Now a new non-dimensional time  $Z$  is introduced:

$$Z = 4 \frac{f_1}{D} \bar{u}_1 t. \quad (39)$$

It is found from Eq. (36) that the velocity reaches the new steady state at  $Z = 3-4$  (Figs. 5 and 6).

### 3.3 Variation of $f/f_{st}$

Figure 7 illustrates the variation of the friction factor ratio  $f/f_{st}$  for various initial and final Reynolds numbers. In case of the acceleration, the ratio  $f/f_{st}$  increases very much as the ratio  $Re_1/Re_0$  increases. In case of very severe transient  $Re = 10^4 \rightarrow 10^6$ , the ratio  $f/f_{st}$  comes up as high as 7.

In case of the deceleration,  $f/f_{st}$  does not differ much from unity. Even in case of the severe transient  $Re = 10^6 \rightarrow 10^4$ , the ratio is only slightly less than unity. The reason will be discussed below.

Figure 8 illustrates the variation of the velocity profile in the case of acceleration. Solid lines are the transient velocity profiles while broken lines are the steady state velocity profiles. The mean velocities of both lines are equal.

One can see that the transient velocity profile is flatter than the steady state one in the central region and is steeper near the wall. The two terms on the right hand side of Eq. (5) are equal in the initial steady state. Then, the first term in the right hand side, i.e. the pressure drop term, increases stepwisely in case of the acceleration. To accelerate the flow from  $Re = 10^4$  to  $10^5$ , the

pressure drop must increase roughly by a factor of 50. The second term is nearly negligible compared to the first term at the initial moment of the transient.

The flow is accelerated nearly uniformly in the central region. So, the velocity profile becomes relatively flat in the center. On the other hand, the velocity is kept zero at the wall, then the velocity profile cannot but be steep near the wall. This is the reason why the friction factor is larger than its steady state value in case of the acceleration.

Figure 9 shows the variation of the velocity profile in the case of deceleration. The velocity profile is nearly equal to the steady state profile; so the friction factor is also nearly equal to its steady state value.

In case of the deceleration, the pressure drop term in Eq. (5) is negligible compared with the second term on the right hand side, i.e. the friction term. The decay of the flow is determined by its friction itself.

This means that the steady state velocity profile is retained if a turbulent flow decays by itself. A further study is needed for this point.

#### 3.4 Comparison with the quasi-static calculation

The present interest lies rather in the validity of the quasi-static equation than in the variation of the friction factor. The solution of the quasi-static momentum equation  $\bar{u}_{\text{quasi}}$  is compared with the mean velocity  $\bar{u}$  obtained from the two-dimensional momentum equation in Fig. 10. The ratio  $\bar{u}_{\text{quasi}}/\bar{u}$  is very close to unity in case of acceleration; while it deviates nearly 5 - 10 % from unity in case of deceleration.

In acceleration, the friction factor deviates very much from its steady state value; nevertheless, the velocity variation is nearly quasi-static. This can be explained by comparing the two terms on the right hand side of Eq. (1). These two terms have the same value at the initial state, then the pressure drop term increases much quicker than the friction term. So, the friction factor has a smaller effect on the velocity variation even when it changes much. In other words, the inertia of the fluid is dominant, and the friction is negligible at the initial stage of the transient. As time elapses, the dissipation term becomes important again. At that time, however, the friction factor has already come to its new steady state value. This is the reason why the quasi-static momentum equation is valid in the acceleration.

In case of the deceleration, the friction term is dominant. Only a slight error in the friction factor results in a relatively large error in the velocity calculation. As the error is less than 10 % even in the severest transient of  $Re = 10^6$  to  $10^4$ , one can conclude that the quasi-static assumption is approximately valid in the deceleration, too.

In conclusion, the quasi-static momentum equation is roughly valid for both the acceleration and the deceleration. The error due to the quasi-static assumption is very small in case of the acceleration and is relatively large but less than 10 % in case of deceleration.

#### 4. Transient Heat Transfer

##### 4.1 Variation of heat transfer coefficient

An example of the transient calculation with heat transfer is shown in Fig. 11. The flow is accelerated from  $Re = 10^4$  to  $10^5$ , so the wall temperature difference,  $\Delta T_w = T_w - \overline{T}_f$ , decreases. The heat transfer coefficient ratio  $\alpha/\alpha_{st}$  decreases down to about 0.6 and then comes back to 1. An example of deceleration is shown in Fig. 12. The heat transfer coefficient does not deviate much in case of deceleration.

Figure 13 shows the variation of  $\alpha/\alpha_{st}$  for various initial and final Reynolds numbers. The heat transfer coefficient ratio  $\alpha/\alpha_{st}$  depends very much upon the initial and final Reynolds numbers in case of the acceleration. In case of the deceleration, however, it does not depend much upon the initial and the final Reynolds numbers and it is always near to unity.

#### 4.2 Case of deceleration

The variation of  $\Delta T_{w,quasi}/\Delta T_w$  and  $\alpha/\alpha_{st}$  are illustrated in Fig. 14. Here,  $\Delta T_{w,quasi}$  is obtained from the quasi-static equations (29)-(31), while  $\Delta T_w$  is obtained from the two-dimensional equations (5) and (6).

The parameter  $\beta$  is a non-dimensional number pertinent to the wall heat capacity. It is defined as follows:

$$\beta = 4 f_1 Re_1 \frac{\bar{H} Pr}{Nu_1} \quad (40)$$

This parameter has been derived rather intuitively than mathematically. Its physical meaning is

$$\beta \propto \frac{\left[ \begin{array}{l} \text{time for } T_w \text{ to reach steady state in} \\ \text{case of a large wall heat capacity.} \end{array} \right]}{\left[ \text{time for } \bar{u} \text{ to reach steady state} \right]} \quad (41)$$

Fig. 14 shows that  $\alpha/\alpha_{st}$  is slightly dependent while  $\Delta T_{w,quasi}/\Delta T_w$  is more dependent on the wall heat capacity. The error in the quasi-static  $\Delta T_w$  is due to the combined effects of both errors in  $\bar{u}$  and in  $\alpha$ . When the wall heat capacity  $\beta$  becomes larger, the error in  $\Delta T_{w,quasi}$  becomes smaller. The error is almost 15 % even when  $\beta = 0$ . Figure 14 shows a severe transient from  $Re = 10^6$  to  $10^4$ . The same tendency can be obtained in all other decelerations.

The difference between the wall and the mean fluid temperature is dominant to determine the wall temperature in case of cooling by normal fluids. However, the variation of the mean fluid temperature

was examined too, and the ratio  $(\bar{T}_f - T_{in})_{quasi}/(\bar{T}_f - T_{in})$  was also found nearly equal to 1. So, one can conclude that the quasi-static energy equation is approximately valid in case of the deceleration. Moreover, the quasi-static assumption results in a slightly higher wall temperature than the actual one. This error is usually on the safe side in reactor accident analyses.

This conclusion is of importance because the flow deceleration is to be solved in almost all the cases of reactor safety analysis.

#### 4.3 Case of acceleration

Figure 15 shows variations of  $\alpha/\alpha_{st}$  for  $\beta = 0$  and 1 at various axial positions for the acceleration from  $Re = 10^4$  to  $10^6$ . The arrow shows the time when a "new fluid" comes to that position; the "new fluid" means that the fluid which was just at the entrance of the heating section at  $t = 0$ . To calculate the arrows, all the fluid is assumed to flow with the mean velocity.

The curve for  $\beta = 0$  is discussed at first. The ratio  $\alpha/\alpha_{st}$  decreases well below 1, and has a plateau. The flow has already come to a new steady state at about  $Z = 4$ , but the plateau continues even after the flow has reached the steady state. The heat transfer coefficient comes back to its steady state value after the "new fluid" has come to that position.

The minimum at the initial stage of the transient does not mean that the heat transfer coefficient itself exhibits a minimum. The ordinate is the heat transfer coefficient ratio  $\alpha/\alpha_{st}$ . At the initial stage of the transient, the flow is accelerated very quickly, so the corresponding steady state heat transfer coefficient  $\alpha_{st}$  increases very quickly. The temperature profile tends to change to match the new velocity profile. However, the temperature profile can not change so quickly partly because the fluid has a finite heat capacity and partly because the thermal eddy diffusivity is small at the first moment.

So, the heat transfer coefficient  $\alpha$  changes relatively slowly compared with  $\alpha_{st}$  at small times. When the time elapses and the flow has been accelerated, the thermal eddy diffusivity near the wall increases. So, the temperature profile can redistribute quickly, and the heat transfer coefficient increases rapidly. This is the reason for the minimum of  $\alpha/\alpha_{st}$  at the initial stage of transient.

The broken line in Fig. 15 shows the variation of  $\alpha/\alpha_{st}$  for  $\beta = 1$ . The general tendency is the same as that of  $\beta = 0$  except that the plateau is very near to unity. The first dip is very remarkable, but this minimum has the same reason as discussed above. One can see again that the heat transfer coefficient reaches its steady state value after the "new fluid" comes to that position.

The transient temperature profiles are compared with the steady state ones in Fig. 16. The ordinate is normalized by the temperature difference between the wall and the mean fluid flow. The figure at  $Z = 4$  shows the temperature profile at the plateau. The flow has been already accelerated up to a new steady state; one can see however that relatively hot fluid still exists near the wall. This tends to decrease the heat transfer coefficient.

The initial thermal sublayer near the wall is thicker than the final one in case of the acceleration. So, the relatively hot layer initially exists upstream and is flowing downstream during the transient. The hot layer near the wall begins to disappear when the "new fluid" comes to that position. This is the reason for  $\alpha/\alpha_{st}$  to reach unity after the "new fluid" has come to that position.

Figure 17 compares the temperature profiles for  $\beta = 0$  and 1 at early times. The ordinate is normalized by the initial wall temperature. In case of  $\beta = 0$ , the wall temperature drops so quickly that the temperature profile near the wall becomes relatively flat. In case of  $\beta = 1$ , the wall temperature drops slowly; so the steep temperature gradient can be retained even if the hot fluid layer still exists

near the wall. This is the reason for the transient heat transfer coefficient to be higher when the wall heat capacity is larger.

As already known from the previous section, the heat transfer coefficient is nearly equal to its steady state value in case of deceleration. In this case, the wall temperature rises during the transient. No hot layer exists initially near the wall. A new temperature profile can develop into the fluid as the wall temperature rises. The temperature profile can develop fast enough in turbulent flow, and the velocity has nearly its steady state profile as known in the previous chapter. So, the temperature has nearly its steady state profile, and the heat transfer coefficient is nearly equal to its steady state value in case of the deceleration.

Figure 18 illustrates the effects of the wall heat capacity  $\beta$  and Prandtl number  $Pr$  upon the variation of  $\alpha/\alpha_{st}$  in the accelerated flow. The variation of  $\alpha/\alpha_{st}$  does not depend much on  $Pr$  if  $\beta > 0$ . Especially, the values of  $\alpha/\alpha_{st}$  at the plateau are nearly equal for different  $Pr$ , holding  $\beta$  constant and assuming that  $\beta > 0$ .

The wall temperature obtained from the quasi-static equation is compared with the one obtained from the two-dimensional equation in Fig. 19. The ordinate is the ratio  $\Delta T_{w,quasi}/\Delta T_w$ , where  $\Delta T_w = T_w - \bar{T}_f$ . When  $\beta \gg 1$ , the ratio is nearly equal to unity independent of  $Pr$ . This figure illustrates the example of the severe acceleration from  $Re = 10^4$  to  $10^6$ . In case of less severe accelerations, the ratio is closer to unity.

The variation of mean fluid temperature was also examined, and was found approximately quasi-static when  $\beta \gg 1$ . So, it can be concluded that the quasi-static energy equation is valid also for acceleration when  $\beta \gg 1$ .

#### 4.4 Liquid metal cooling

The conclusions about the transient hydraulics obtained in chapter 3 are exactly applicable to liquid metal cooling also. Some sample calculations of the transient heat transfer will be given in the present chapter. The steady state heat transfer coefficients are compared in Fig. 20 with two correlations by Lubarsky & Kaufman<sup>(6)</sup>, and Skupinski et al.<sup>(7)</sup>. It can be found in Fig. 20 that  $\epsilon_H$  calculated with Eq. (20) gives a lower heat transfer coefficient than these correlations. So, Eq. (20) is simply doubled to get a better result.

$$\sigma = 3.0 \phi [1 - \exp(-1/\phi)] \quad (42)$$

One can see in Fig. 20 that Eq. (42) gives a better result than Eq. (20).

Examples of transient heat transfer for the flow acceleration and deceleration are shown in Figs. 21 and 22. Each figure contains the transients for  $\hat{H} = 0$  and 0.7. The latter is a plausible value in a LMFBR. The ratio  $(T_w - T_{in})_{quasi} / (T_w - T_{in})$  is plotted in Fig. 21 and 22 instead of  $(T_w - \bar{T}_f)_{quasi} / (T_w - \bar{T}_f)$  in the preceding chapter. The temperature difference  $(T_w - \bar{T}_f)$  is dominant in case of normal fluid cooling. In liquid metal cooling, however,  $(T_w - \bar{T}_f)$  is less dominant than the axial fluid temperature rise  $(\bar{T}_f - T_{in})$  because the heat transfer coefficient is very large.

One can see in Figs. 21 and 22 that the transient variation of the heat transfer coefficient at early times is similar to that of the normal fluid cooling. The ratio  $\alpha/\alpha_{st}$  decreases below unity in the acceleration, while it is a little bit larger than unity in the deceleration. The transient variation of  $\alpha/\alpha_{st}$  at large times is more or less different from that of the normal fluid cooling when  $\hat{H} = 0.7$ . The ratio  $\alpha/\alpha_{st}$  becomes larger than unity in the acceleration while it becomes smaller in the deceleration.

The variation of the ratio  $(T_w - T_{in}) / (T_w - T_{in})$  shows a quite similar tendency as that of the normal fluid cooling. The ratio stays nearer to unity as the wall heat capacity becomes larger. The error in the quasi-static wall temperature is small when  $H = 0.7$ .

Further studies are of course needed for the liquid metal cooling especially for more severe transients and various wall heat capacities.

## 5. Application to Reactors

Some parameters which have been derived in the present analysis are calculated for several types of power reactors. Table 2 lists the time for the flow to reach a new steady state  $t_{st,u}$ , the ratio of heat capacity  $\hat{H}$ , and the non-dimensional heat capacity  $\beta$ . The heat capacity of the clad is included in the wall heat capacity. These numbers are not so precise but give the order of magnitude.

The time required for the flow to reach a new steady state is very short in GCFR and relatively long in PWR. The LMFBR lies in the middle. In GCFR, the flow can follow a change of the pressure drop very quickly. In PWR, a rather large time lag is expected.

The ratio of heat capacity  $\hat{H}$  and the non-dimensional heat capacity  $\beta$  are very large in GCFR. So, the quasi-static energy equation is valid for accelerated and decelerated flows. The reason for  $\hat{H}$  and  $\beta$  to be so large in GCFR is that  $\rho c_p$  of the fuel is much larger than that of the coolant. So, one can expect that the quasi-static energy equation is valid for all gas cooled reactors.

The non-dimensional heat capacity  $\beta$  is nearly 1 in PWR and a little bit less than 1 in LMFBR. The present conclusion has been that the quasi-static energy equation is always roughly valid for deceleration, while it is valid only when  $\beta \gtrsim 1$  for acceleration. So, the quasi-static assumption is roughly valid for deceleration, but these  $\beta$ 's

are rather critical for acceleration. From only the present results, one can expect that the quasi-static assumption will not bring a serious error in PWR and LMFBR. However, the fluid properties vary and the thermal resistance in the fuel can not be neglected. Further studies are needed to get a definite conclusion for these reactors, especially for LMFBR.

## 6. Conclusions

### Transient Hydraulics

- 1) In a decelerated flow, the transient friction factor is slightly less than its steady state value, and quasi-static assumption is roughly valid.
- 2) In an accelerated flow, the friction factor temporarily increases very much. However, a correct flow variation can be obtained from the quasi-static momentum equation.
- 3) The quasi-static momentum equation is approximately applicable to both the accelerated and the decelerated flows. The error due to the quasi-static assumption is larger in case of deceleration.

### Transient heat transfer

- 4) In a decelerated flow, the transient heat transfer coefficient is a little bit larger than its steady state value, and quasi-static assumption is roughly valid.
- 5) In an accelerated flow, the transient heat transfer coefficient decreases well below its steady state value if the heating wall has no heat capacity. When the wall has a large heat capacity, the heat transfer coefficient does not decrease so much and the quasi-static assumption is approximately valid.

- 6) The quasi-static energy equation can be applied to flow acceleration and deceleration of GCFRs.

The present conclusions are concerning the flow transient in the turbulent region. A further study is needed for the flow transient from turbulent region to laminar and/or transition region. The effect of property variation and the case of liquid metal cooling need to be investigated further.

#### Acknowledgements

The author would like to express his gratitude to Prof. Dr. K. Wirtz for his interest in the present work, and to Dr. M. Dalle Donne and Dr. K. Rehme for their helpful discussions. The author wishes also to thank Mr. D. Wilhelm and Mr. L. Meyer for their great helps and Mrs. Lott for typewriting the manuscript.

Nomenclature

$A^+$	damping factor
$\alpha$	thermal diffusivity $m^2/sec$
$c_p$	specific heat capacity, $kcal/kg_m \text{ deg}$
$D$	diameter of a tube, $m$
$d_w$	thickness of a heating wall, $m$
$f$	friction factor
$g_c$	standard acceleration $kg_m/kg_f \cdot m/sec^2$
$Nu$	Nusselt number $\alpha D/\lambda_f$
$H$	wall heat capacity per unit heat transfer surface,
$\gamma$	heat capacity ratio, Eq. (25)
$\ell$	mixing length, $m$
$P$	pressure, $kg_f/m^2$
$Pr$	Prandtl number = $\nu_f/\alpha_f$
$q_G$	heat generation rate per unit heat transfer surface, $kcal/m^2 \text{ sec}$
$q_n$	net heat flux to fluid, $kcal/m^2 \text{ sec}$
$Re$	Reynolds number = $\bar{u}D/\nu_f$
$r$	radius, $m$
$T$	temperature, $deg, ^\circ C$
$\bar{T}_f$	mixed mean temperature of fluid, $deg, ^\circ C$
$t$	time, $sec$
$u$	velocity, $m/sec$
$\bar{u}$	mean velocity $m/sec$
$u^*$	friction velocity = $\sqrt{g_c \tau/\rho_f}$ , $m/sec$
$x$	axial distance, $m$
$y$	distance from a wall, $m$
$z$	non-dimensional time, Eq. (39)

Greek

$\alpha$ :	heat transfer coefficient
$\beta$ :	non-dimensional wall heat capacity, Eq. (40)
$\epsilon_H$ :	Thermal eddy diffusivity, $m^2/sec$
$\epsilon_M$ :	momentum eddy diffusivity, $m^2/sec$
$\lambda$ :	thermal conductivity, kcal/m sec deg
$\lambda_\ell$ :	coefficient in the mixing length
$\nu$ :	kinematic viscosity of fluid, $m^2/sec$
$\rho$ :	density, $kg_m/m^3$
$\tau$ :	wall shear stress, $kg_f/m^2$

Subscripts

f :	fluid
in:	inlet
$\ell$ :	mixing length
quasi:	quasi-static solution
st:	steady state
w :	heating wall
0 :	initial
1 :	final

References

- (1) Sparrow, E.M. and Siegel, R., Trans. ASME, Ser. C, 82-3 (1960), p. 170.
- (2) Soliman, M., SAN-1011 (1966).
- (3) Kawamura, H., Heat Transfer - Japanese Research, 3 - 1, (1974), p. 45.
- (4) Patanker, S.V. and D.B. Spalding, "Heat and Mass Transfer in Boundary Layers", 2nd ed. (1970), p. 20, Intertext Books, London.
- (5) Mizushima, T., Jour. Japan Soc. Mech. Engirs., 72, (1969), p. 328, (in Japanese).
- (6) Lubarsky, B. and S.J. Kaufman, NACA TN 3336, (1955).
- (7) Skupinski, E. et al., Int. J. of Heat Mass Transfer, 8 - 6 (1965), p. 937.
- (8) Simon, R.H., et al. CONF-740501 Paper 5-3, (1974).
- (9) Directory of Nuclear Reactors, Vol. IV, (1962), IAEA.
- (10) Design Studies of a 1000-MWe Fast Reactor, Power Reactor Technology, 8 - 2 (1964/65), p. 147.

Appendix A Non-dimensional formula

Equations in chapter 2 are transformed into non-dimensional forms. New non-dimensional variables are

$$R = r/D \quad (A-1)$$

$$X = x/D \quad (A-3)$$

$$\tau = t\nu/D^2 \quad (A-4)$$

$$Y = y/D = 1 - R \quad (A-5)$$

$$U = uD/\nu \quad (A-6)$$

$$\theta = \lambda_f T / (Dq_G) \quad (A-7)$$

$$Q_n = q_n/q_G \quad (A-8)$$

Transformed formulae are listed below with the equation number in the text.

$$\frac{\partial U}{\partial \tau} = \beta_x + \frac{1}{R} \frac{\partial}{\partial R} [(E_M + 1) R \frac{\partial U}{\partial R}] \quad (5), \quad (A-9)$$

$$\frac{\partial \theta}{\partial \tau} + U \frac{\partial \theta}{\partial X} = \frac{1}{R} \frac{\partial}{\partial R} [(E_M + \frac{1}{Pr}) R \frac{\partial \theta}{\partial R}] \quad (6), \quad (A-10)$$

$$E_M = \epsilon_M/\nu \quad (A-11)$$

$$E_H = \epsilon_H/\nu \quad (A-12)$$

at  $R = 0.5$

$$U = 0 \quad (7), \quad (A-13)$$

$$\theta = \theta_w \quad (8), \quad (A-14)$$

$$Q_n = \frac{\partial \theta}{\partial R} / R = 0.5 \quad (9), \quad (A-15)$$

$$Q_n = 1 - \tilde{H} \text{Pr} \frac{\partial \theta}{\partial \tau} \quad (10), \quad (A-16)$$

$$\tilde{H} = \frac{H}{(\rho c_p)_f D} \quad (A-17)$$

at  $R = 0$

$$\frac{\partial U}{\partial R} = 0 \quad (11), \quad (A-18)$$

$$\frac{\partial \theta}{\partial R} = 0 \quad (12), \quad (A-19)$$

at  $X = 0$

$$\theta = 0 \quad (13), \quad (A-19)$$

The pressure drop term in Eq. (A-9) is

$$\tilde{P}_x = \begin{cases} 2 f_0 \text{Re}_0^2 & \tau \leq 0 \\ 2 f_1 \text{Re}_1^2 & \tau > 0 \end{cases} \quad (19), \quad (A-20)$$

Eddy diffusivities are:

$$E_M = L^2 \left| \frac{\partial U}{\partial R} \right| \quad (15), \quad (A-21)$$

$$L = \ell / D \quad (A-22)$$

$$L_c = \ell_c / D = \lambda_\ell \quad (16), \quad (A-23)$$

$$L_w = \ell_w / D = \kappa_\ell Y [1 - \exp(-y^+ / A^+)] \quad (17), \quad (A-24)$$

$$y^+ = Y \sqrt{\left| \frac{\partial U}{\partial Y} \right|_{Y=0}} \quad (A-25)$$

$$L^{-2} = L_c^{-2} + L_w^{-2} \quad (18) \quad (A-26)$$

$$L \left| \frac{\partial U}{\partial Y} \right| = \lambda u, \quad \text{if } L \left| \frac{\partial U}{\partial Y} \right| \leq \lambda u \quad (19), \quad (\text{A-27})$$

$$E_H = \sigma E_M \quad (\text{A-28})$$

Quasi-static equations are:

$$\frac{\partial U}{\partial \tau} = \gamma \text{Pr} - 2 f_{st} \bar{U}^2 \quad (29), \quad (\text{A-29})$$

$$\frac{\partial \bar{\theta}_f}{\partial \tau} + \bar{u} \frac{\partial \bar{\theta}_f}{\partial X} = \frac{4}{\text{Pr}} \text{Nu}_{st} (\theta_w - \bar{\theta}_f) \quad (30), \quad (\text{A-30})$$

$$\text{Nu} (\theta_w - \bar{\theta}_f) = 1 - \gamma \text{Pr} \frac{\partial \theta_w}{\partial \tau} \quad (31), \quad (\text{A-31})$$

$$X = 0: \quad \bar{\theta}_f = 0 \quad (32), \quad (\text{A-32})$$

Table 1 Difference formula of the Laplace operator for unequal radial mesh

$$\frac{1}{r} \frac{\partial}{\partial r} \left[ E_r \frac{\partial \phi}{\partial r} \right] = A_k \phi_{k+1} + B_k \phi_{k-1} - D_k \phi_k$$

$$A_k = \left[ E_p D_m + \frac{E_k R + E_k Z}{r_k} M^* \right] / (\Delta r_p \Delta r_m)$$

$$B_k = \left[ E_m D_p - \frac{E_k R - E_k Z}{r_k} P^* \right] / (\Delta r_p \Delta r_m)$$

$$D_k = \left[ E_p D_m M^* + E_m D_p P^* - (P^* - M^*) \left( E_k Z + \frac{E_k R}{r_k} \right) \right] / (\Delta r_p \Delta r_m)$$

$$\Delta r_p = r_{k+1} - r_k, \quad \Delta r_m = r_k - r_{k-1}$$

$$E_p = (E_{k+1} + E_k) / 2, \quad E_m = (E_k + E_{k-1}) / 2$$

$$D_p = 2 \Delta r_p / (\Delta r_m + \Delta r_p), \quad D_m = 2 \Delta r_m / (\Delta r_m + \Delta r_p)$$

$$P^* = \Delta r_p / \Delta r_m, \quad R = \Delta r_p \Delta r_m / (\Delta r_m + \Delta r_p)$$

$$M^* = \Delta r_m / \Delta r_p, \quad Z = 2(\Delta r_p - \Delta r_m) / (\Delta r_m + \Delta r_p)$$

Table 2 Transient parameters for reactors.

Reactor type	GCFR <sup>(*)</sup>		PWR <sup>(**)</sup>		LMFBR <sup>(***)</sup>	
	$10^4$	$10^5$	$10^4$	$10^5$	$10^4$	$10^5$
Final Reynolds number, $Re_1$	$10^4$	$10^5$	$10^4$	$10^5$	$10^4$	$10^5$
Steady state time for $\bar{u}$ , $t_{st,u}$ (sec)	0.14	0.023	7.0	1.2	1.8	0.31
Heat capacity ratio, $\hat{H}$	2.3		0.67		0.71	
Non-dimensional heat capacity $\beta$	150	140	1.6	1.5	0.20	0.85

(\*) GA 300 MWe demonstration plant<sup>(8)</sup>

(\*\*) Indian Point<sup>(9)</sup>

(\*\*\*) GE 1000 MWe design study<sup>(10)</sup>

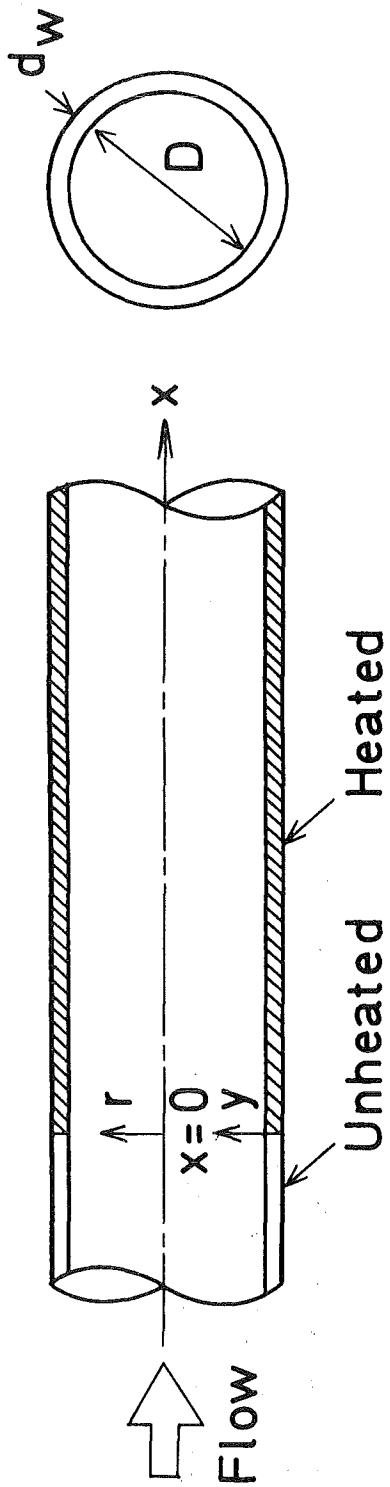


Fig. 1 Co-ordinate.

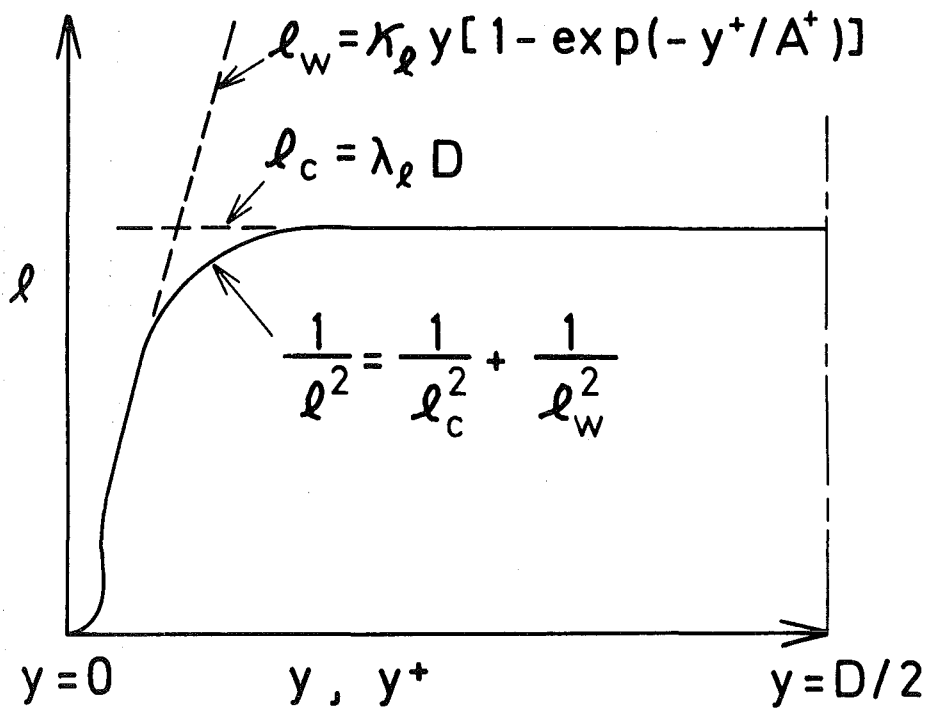


Fig. 2 Mixing length.

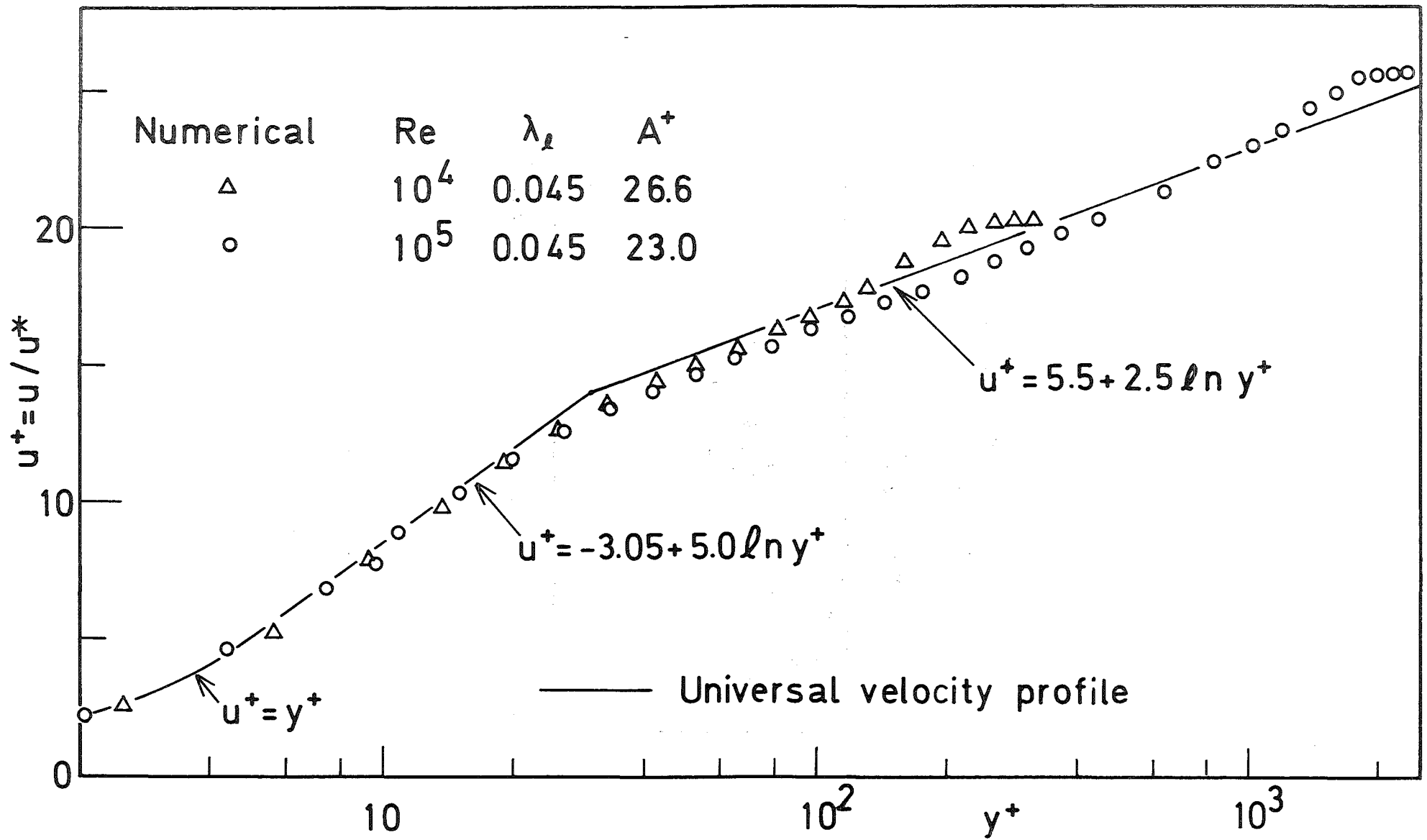


Fig. 3 Velocity distribution in the steady state.

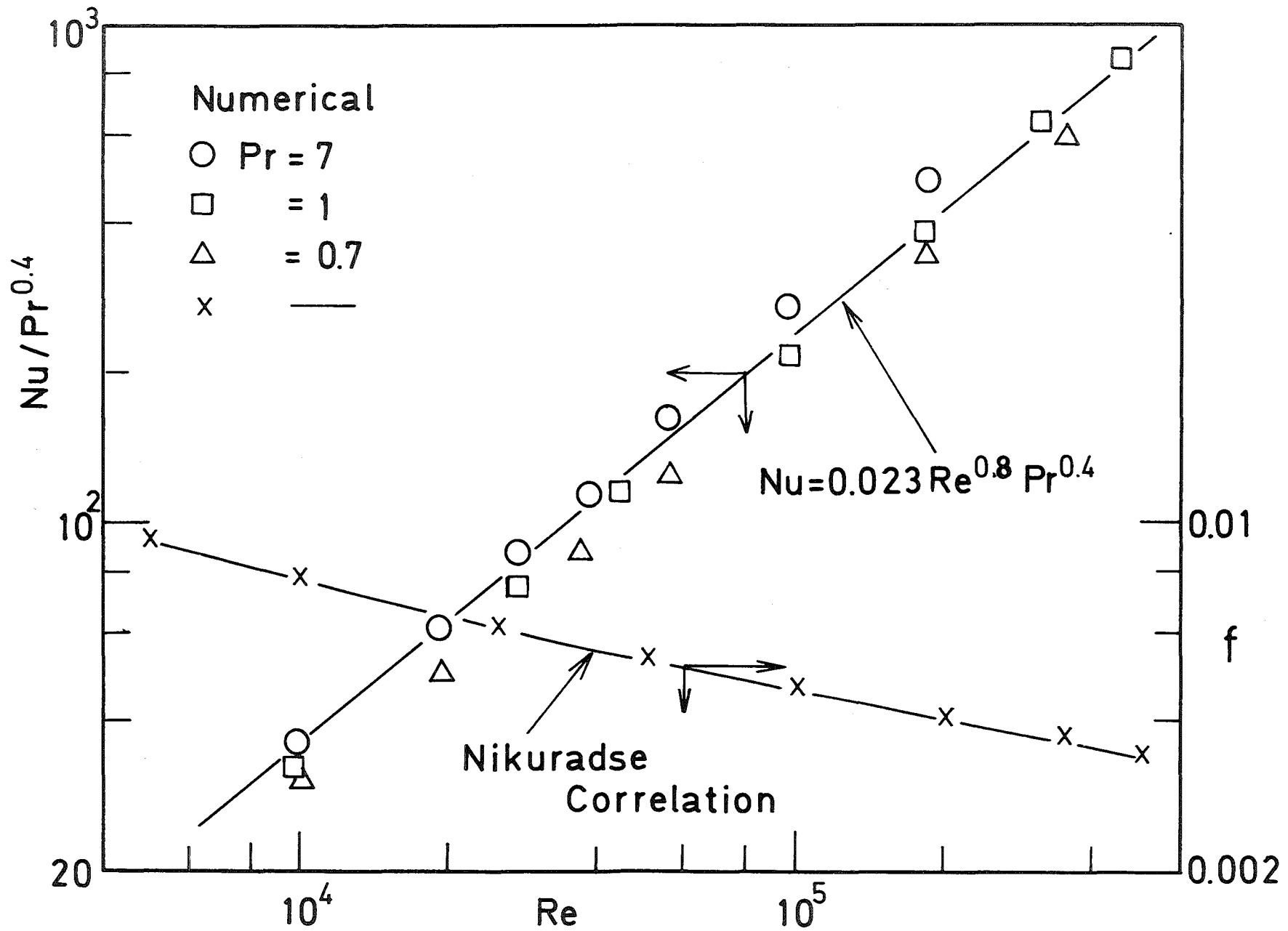


Fig. 4 Heat transfer coefficient and friction factor in the steady state.

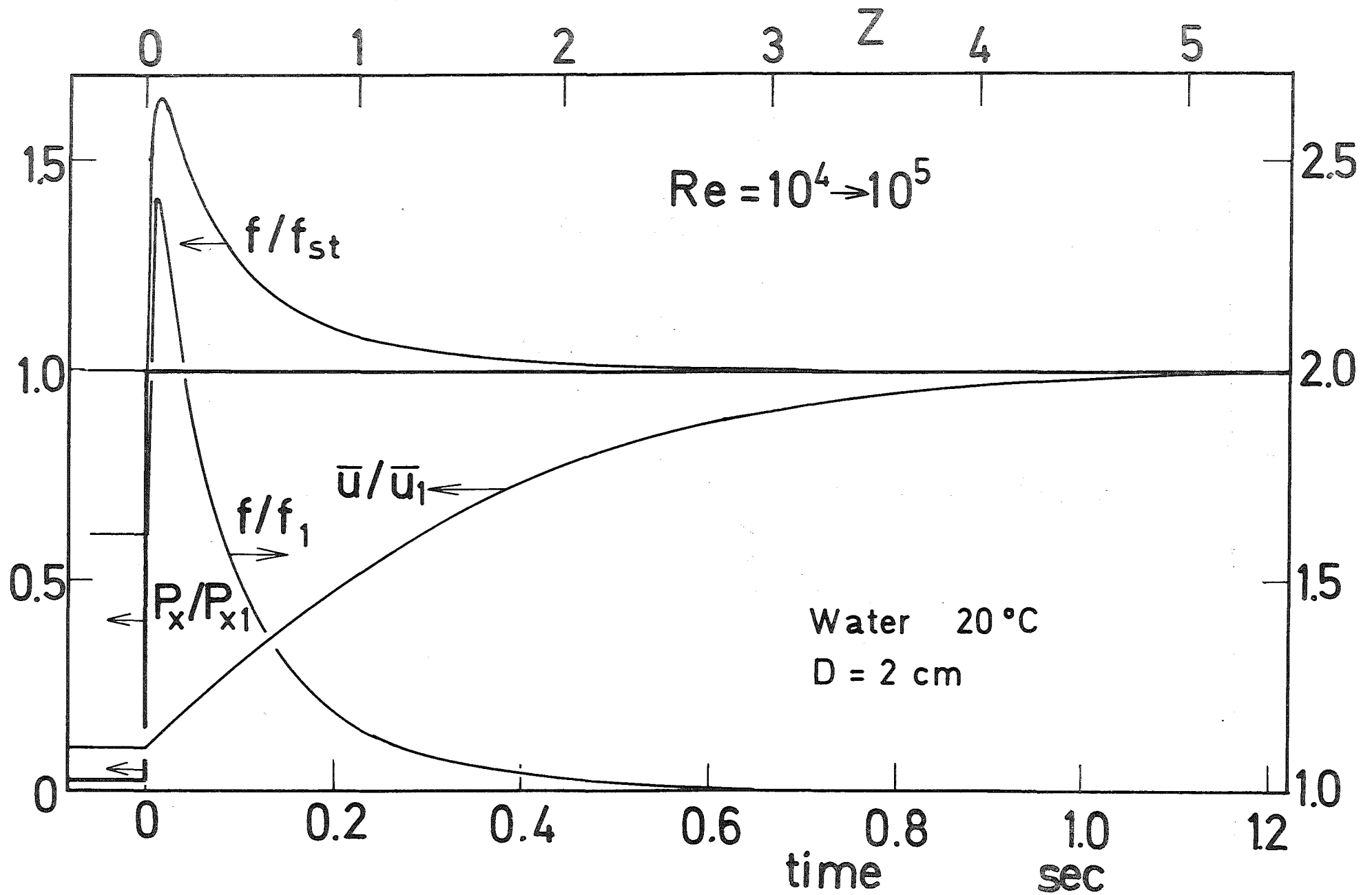


Fig. 5 An example of accelerated transient flow.

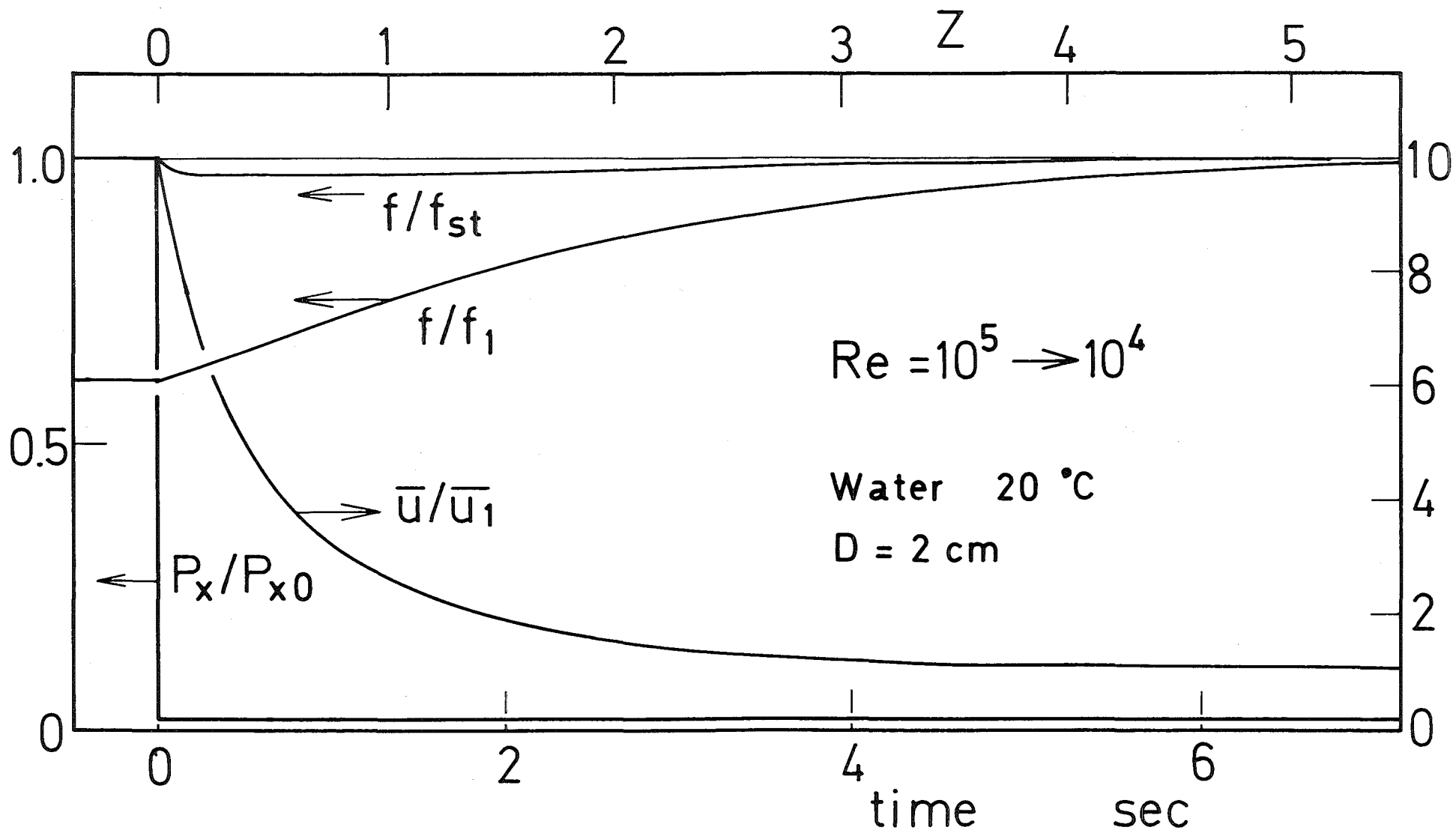


Fig. 6 An example of decelerated transient flow.

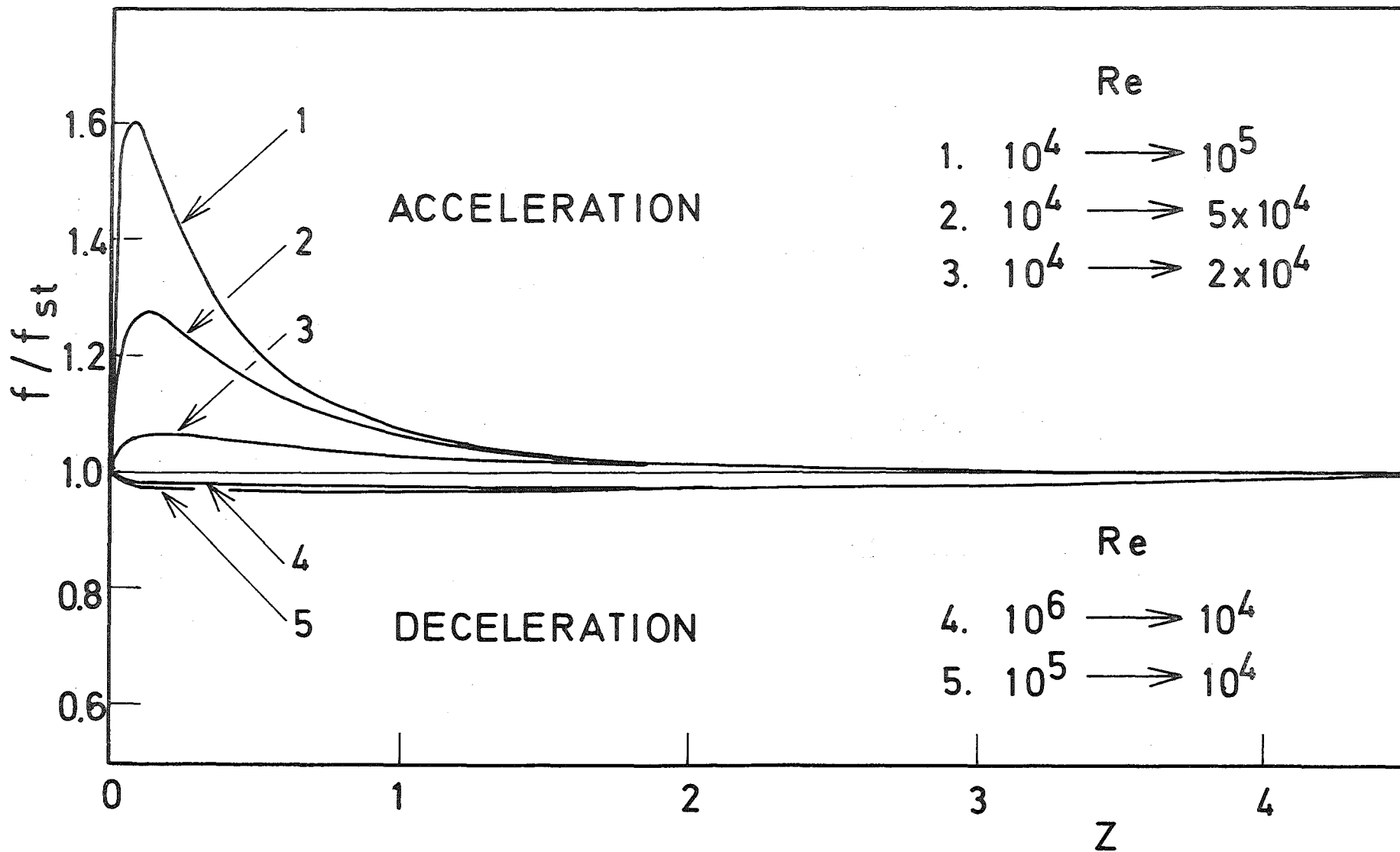


Fig. 7 Transient variation of the friction factor.

# ACCELERATION

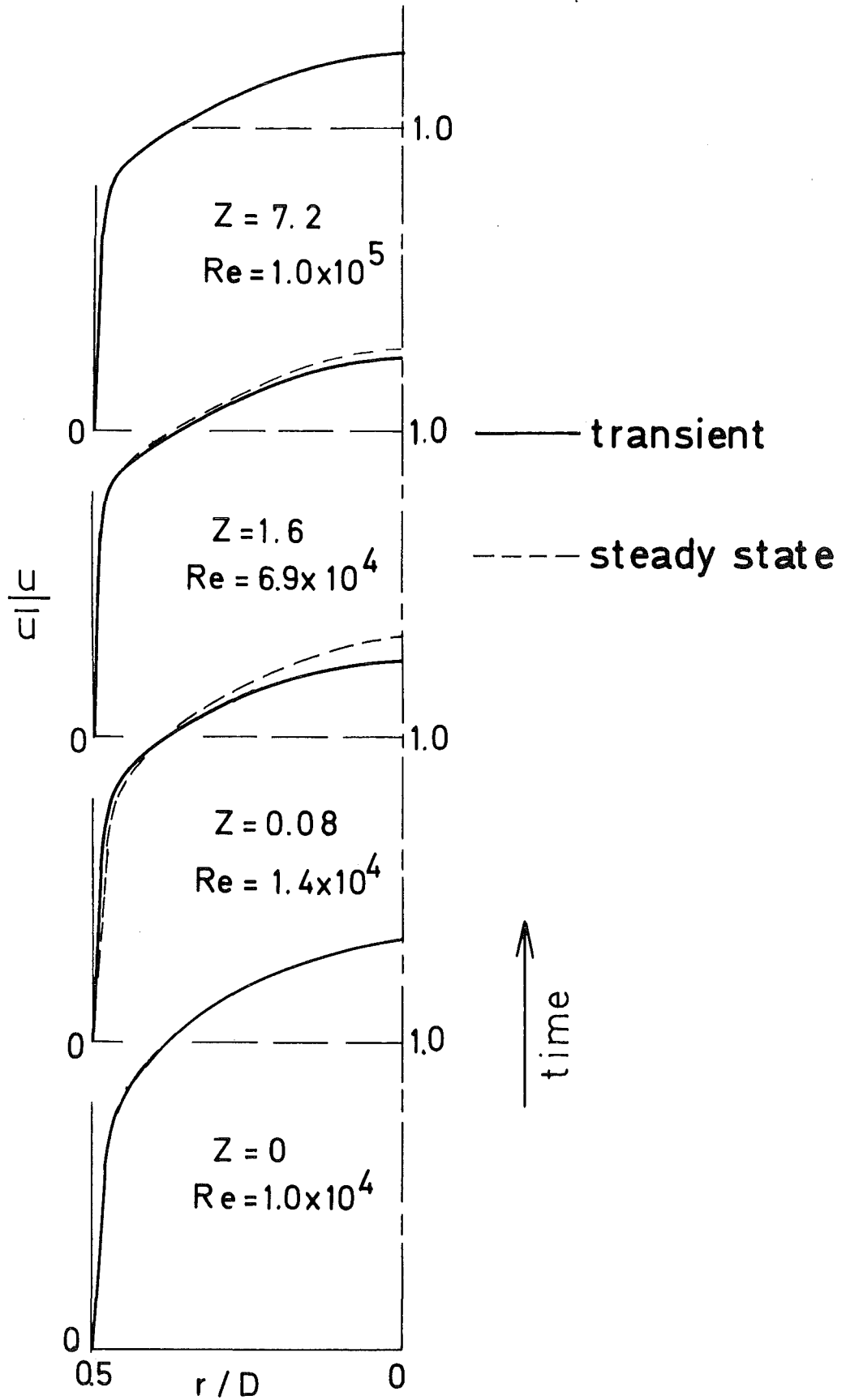


Fig. 8 Transient variation of the velocity profile (accelerated flow).

# DECELERATION

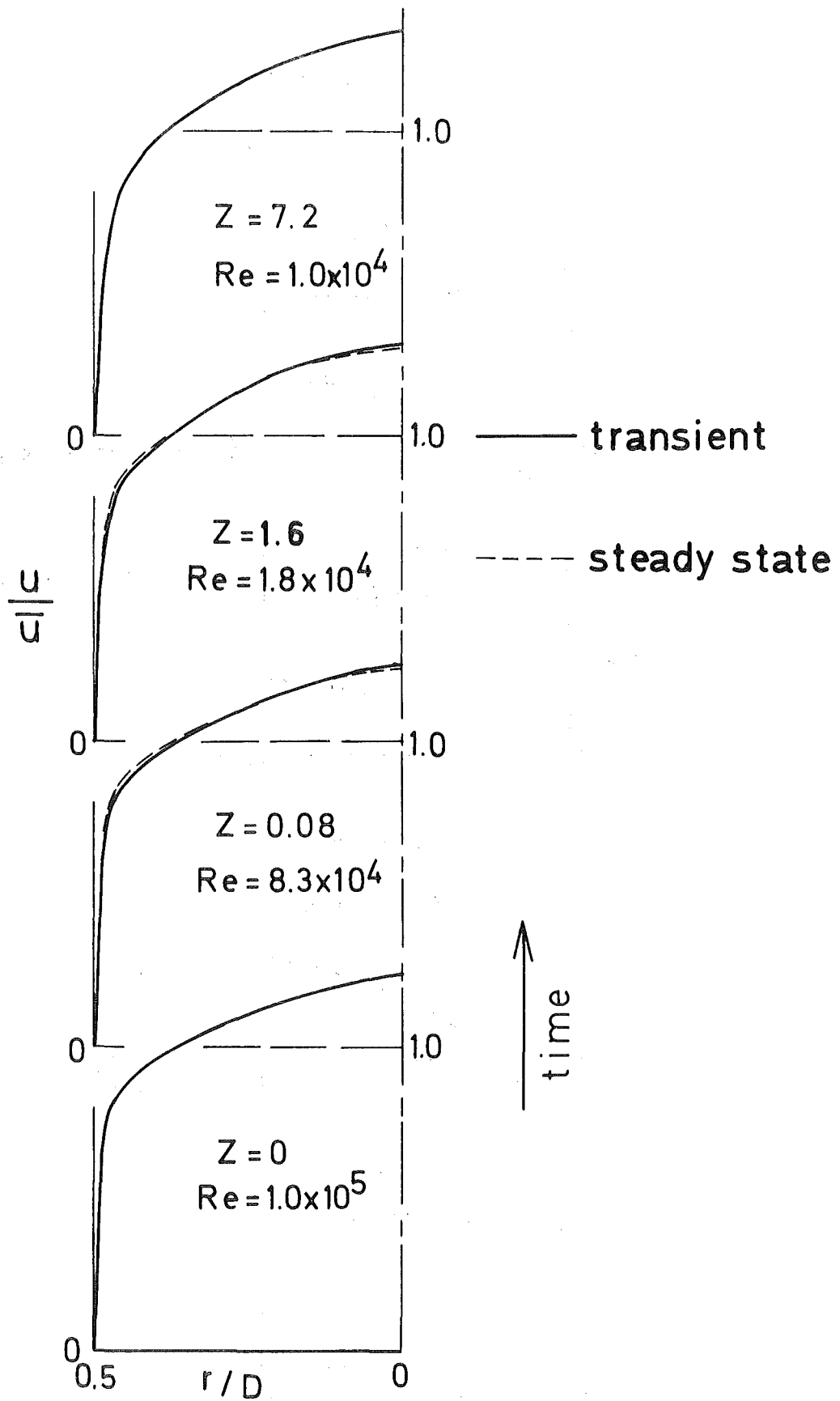


Fig. 9 Transient variation of the velocity profile (decelerated flow).

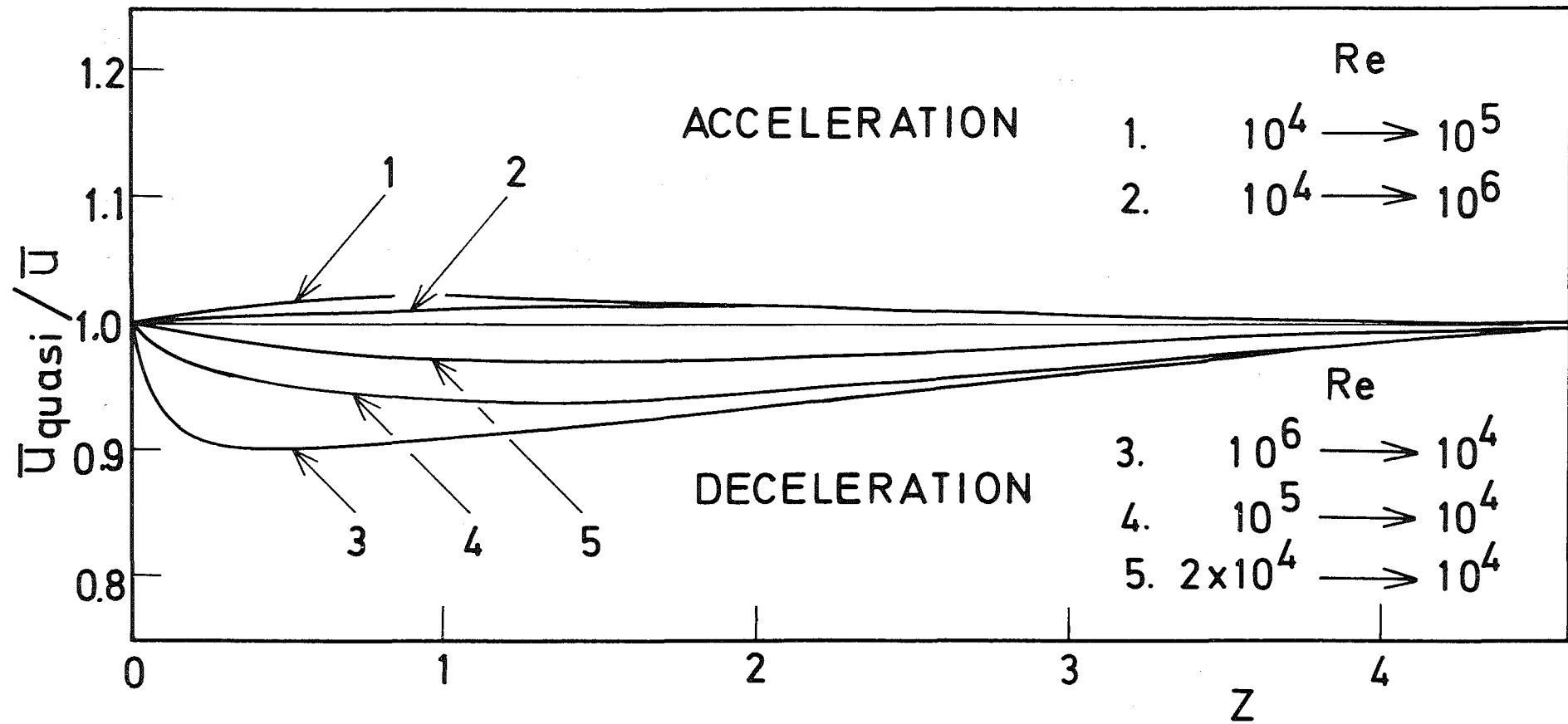


Fig. 10 Variation of  $\bar{u}_{quasi}/\bar{u}$ .

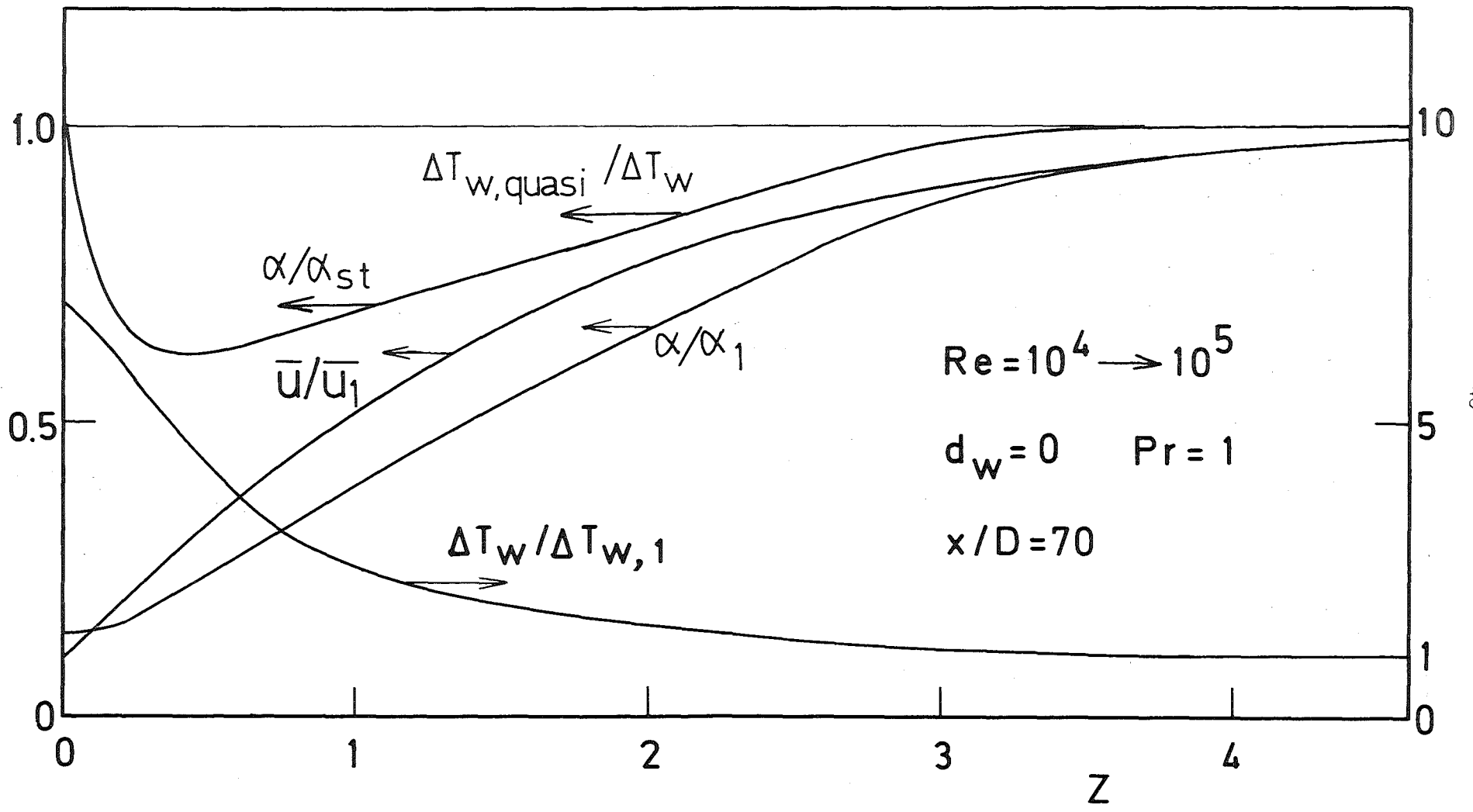


Fig. 11 An example of the transient heat transfer (accelerated flow).

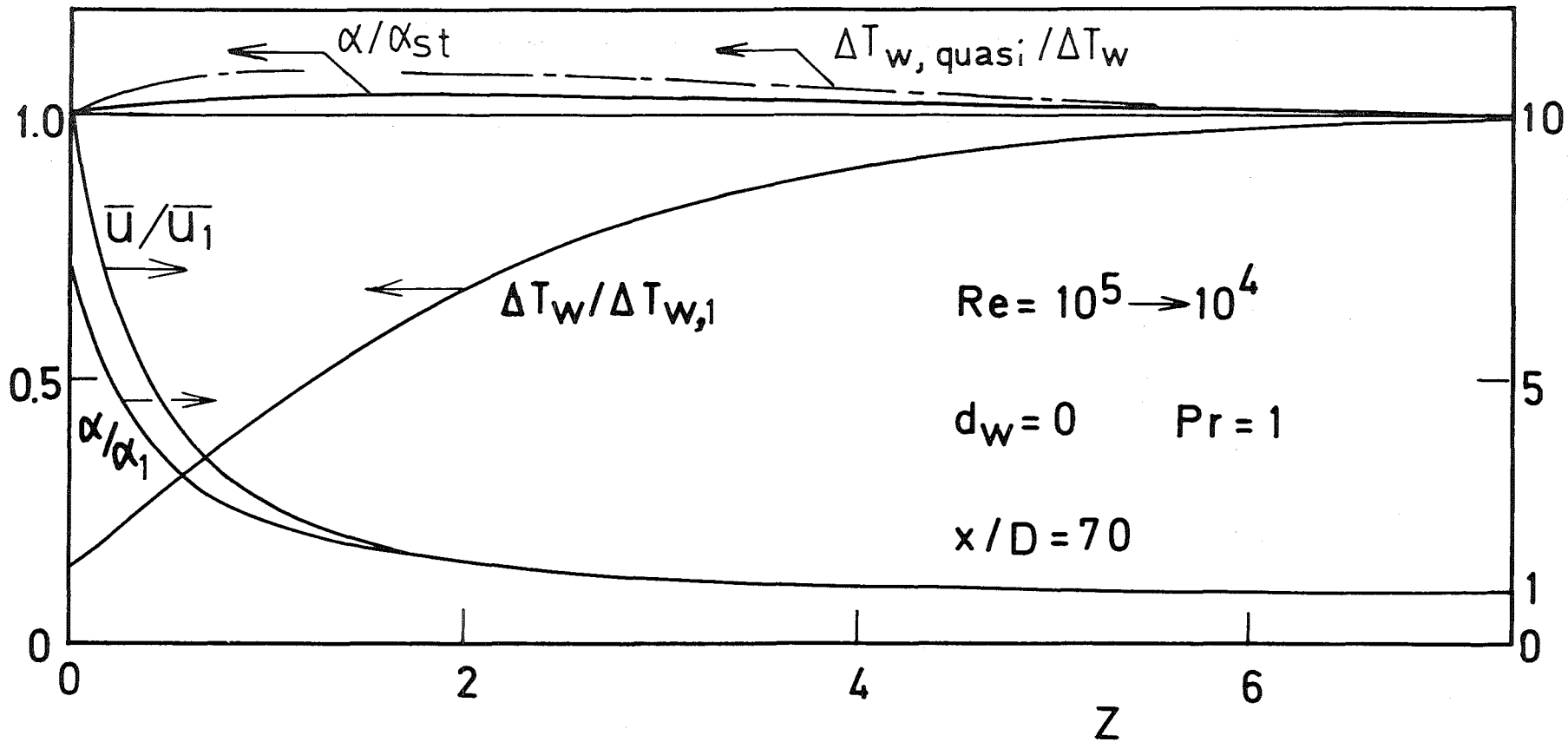


Fig. 12 An example of the transient heat transfer (decelerated flow).

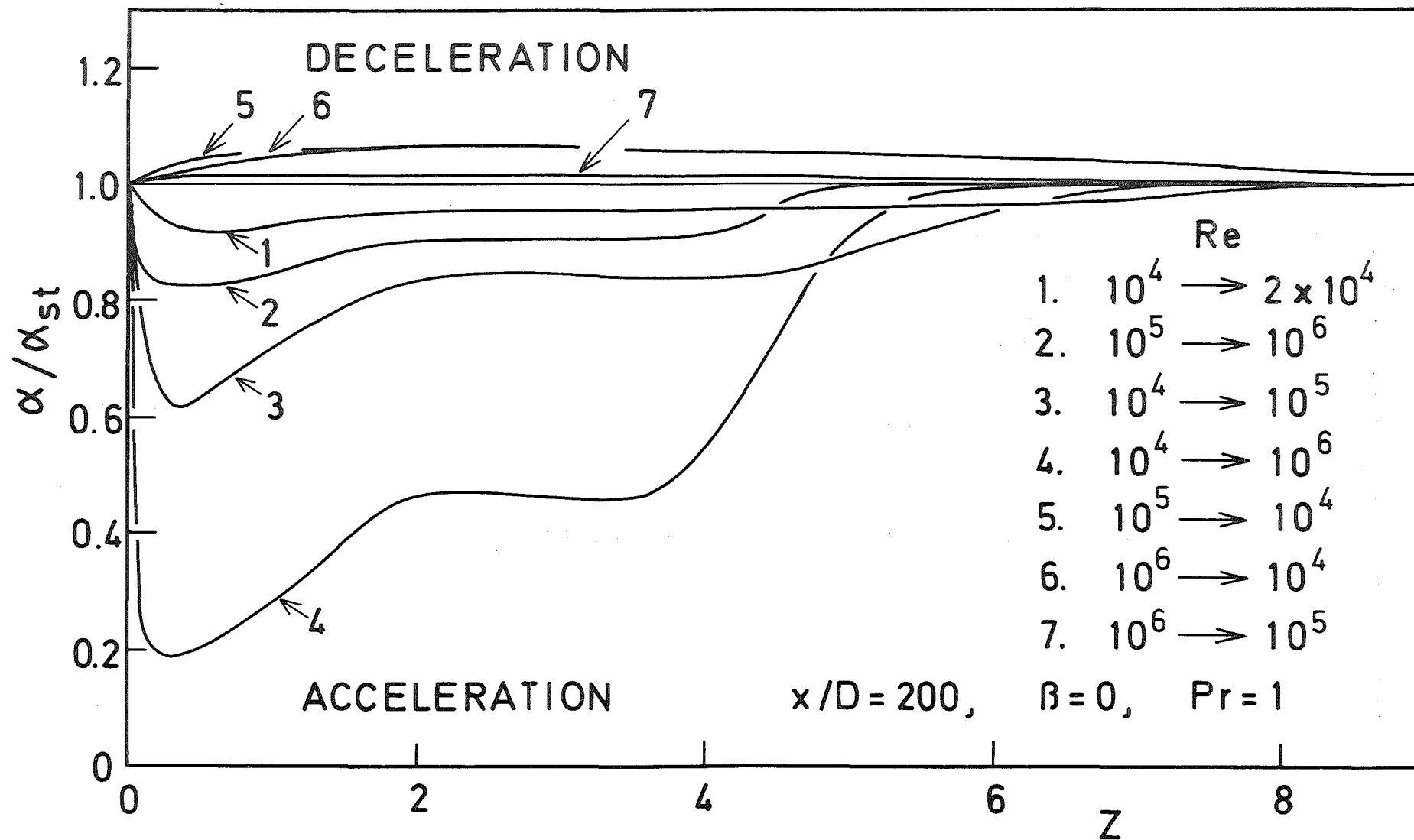


Fig. 13 Variation of  $\alpha/\alpha_{st}$ .

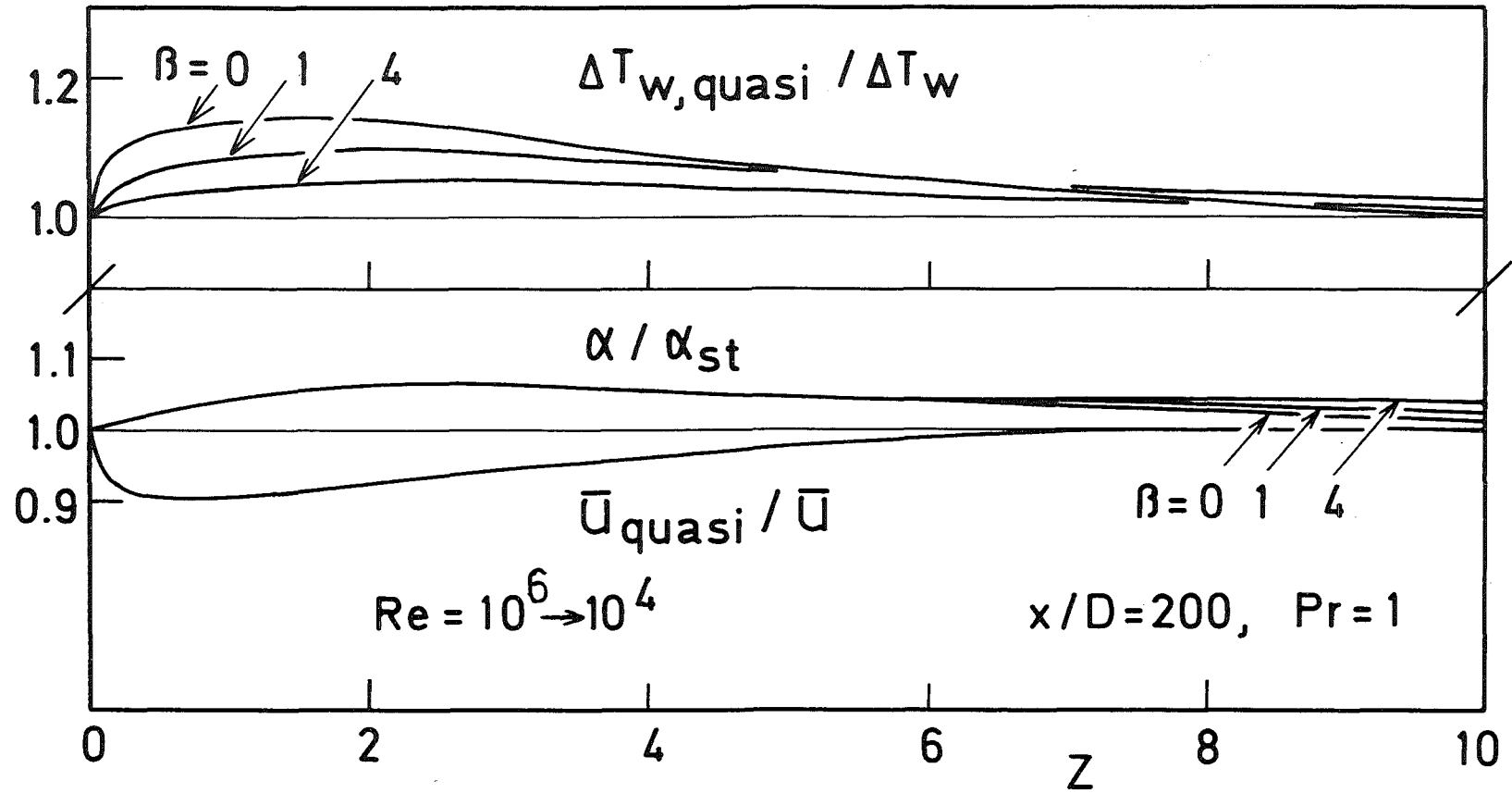


Fig. 14 Variation of  $\alpha/\alpha_{st}$  and  $\Delta T_{w,quasi}/\Delta T_w$  in decelerated flow.

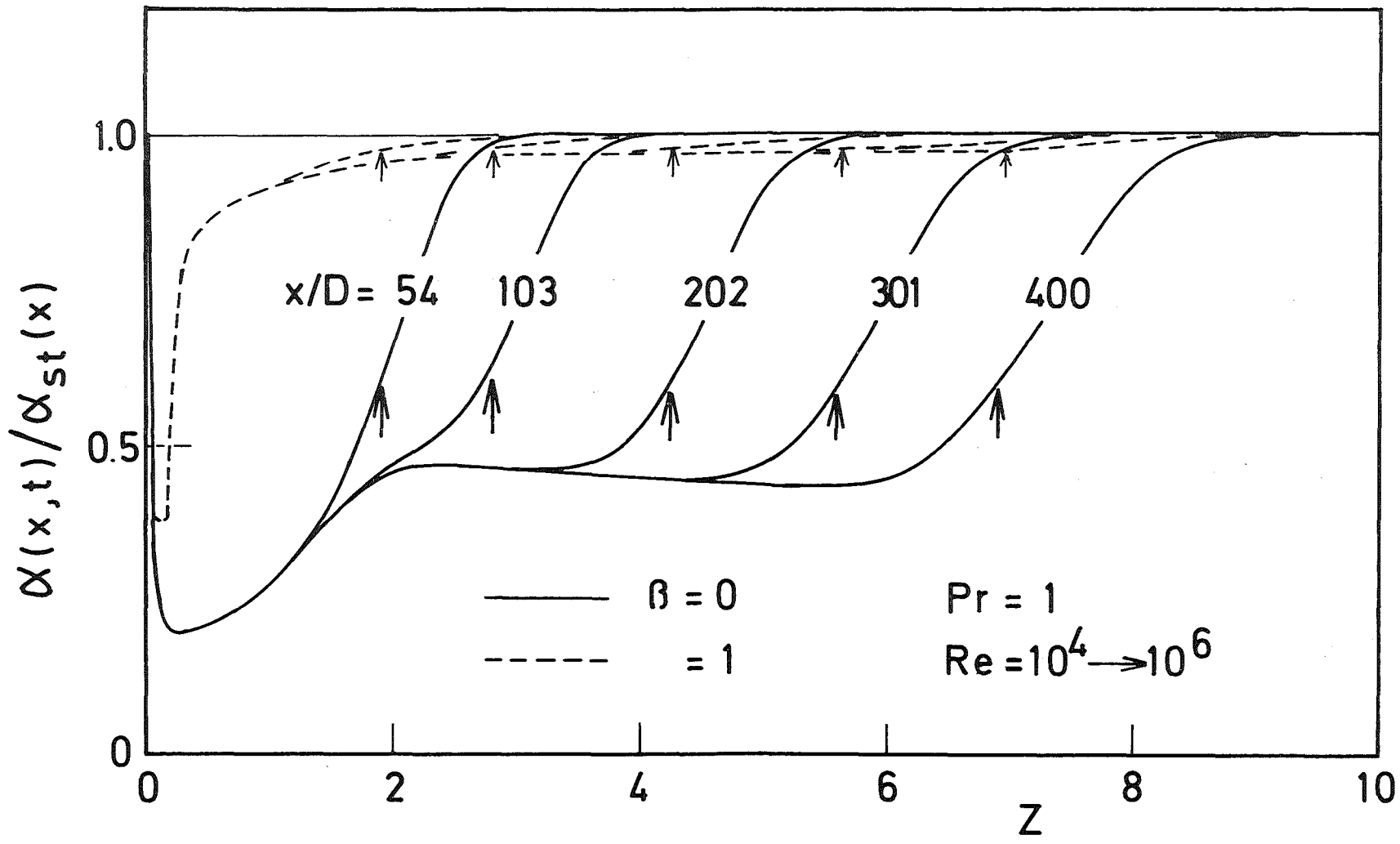


Fig. 15 Variation of  $\alpha/\alpha_{st}$  at various axial positions in accelerated flow.

$Re = 10^4 \rightarrow 10^6, x/D = 400, Pr = 1, \beta = 0$

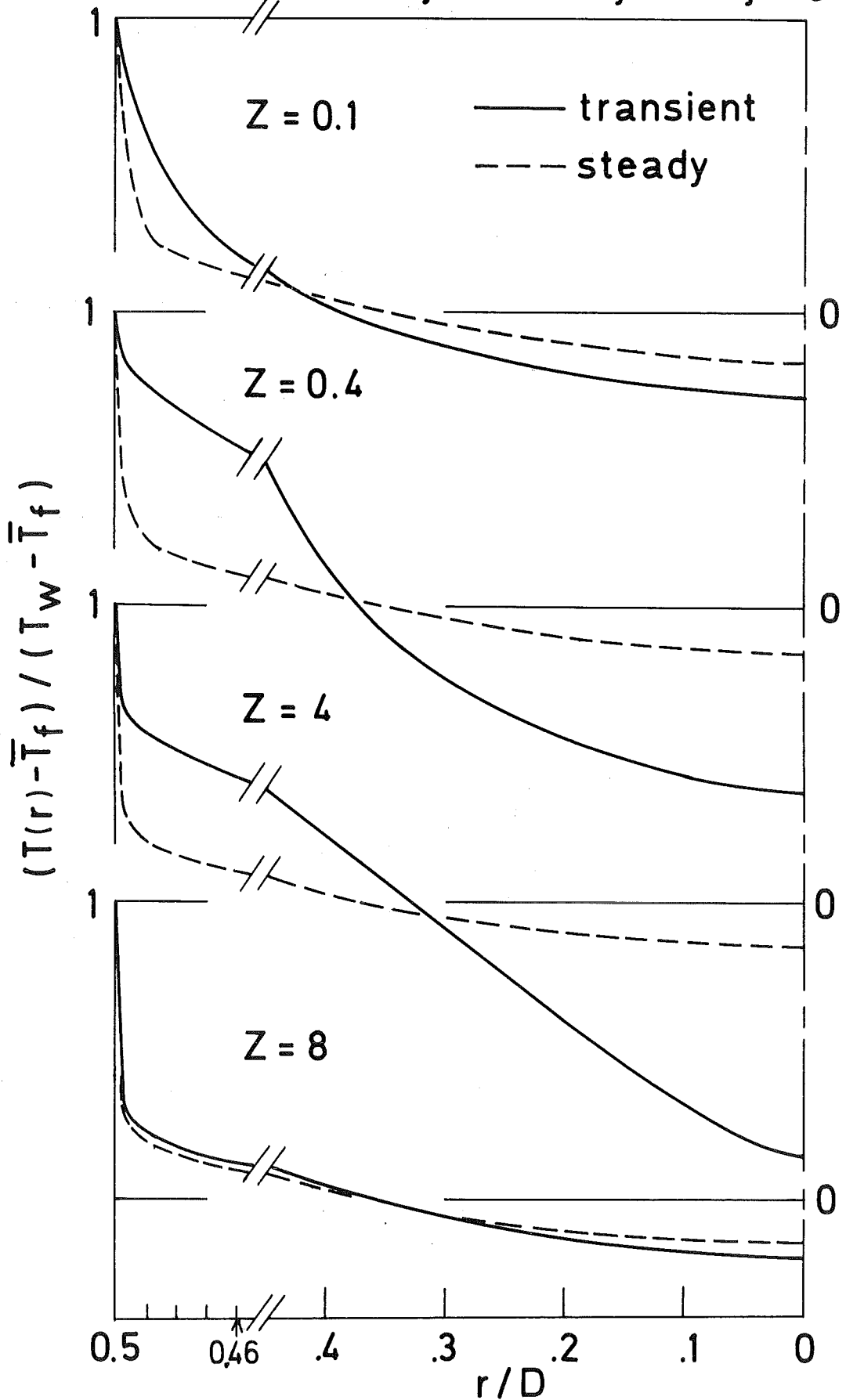


Fig. 16 Variation of the transient temperature profile in accelerated flow.

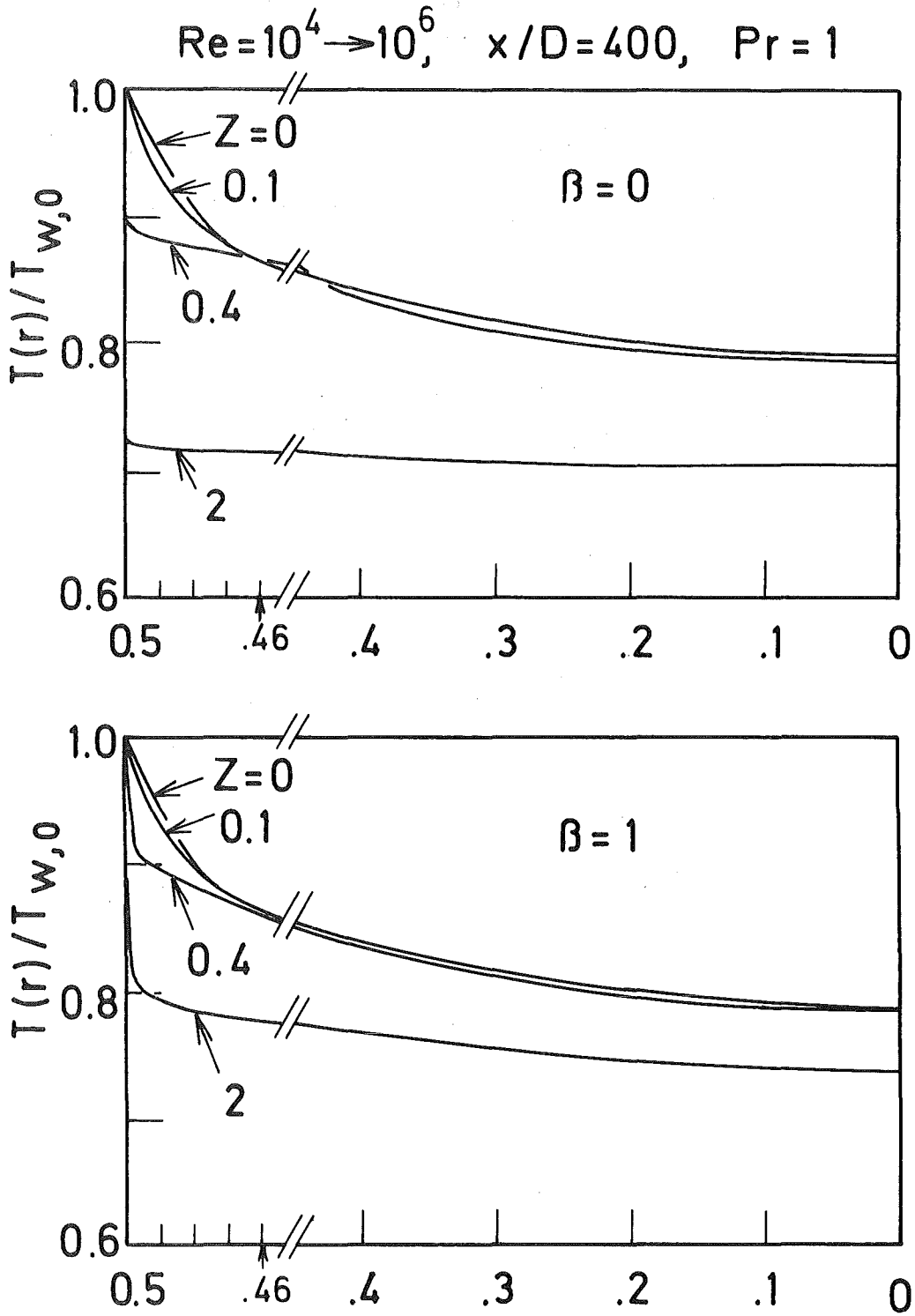


Fig. 17 Variation of the transient temperature profile at early time for  $\beta = 0$  and 1 (accelerated flow).

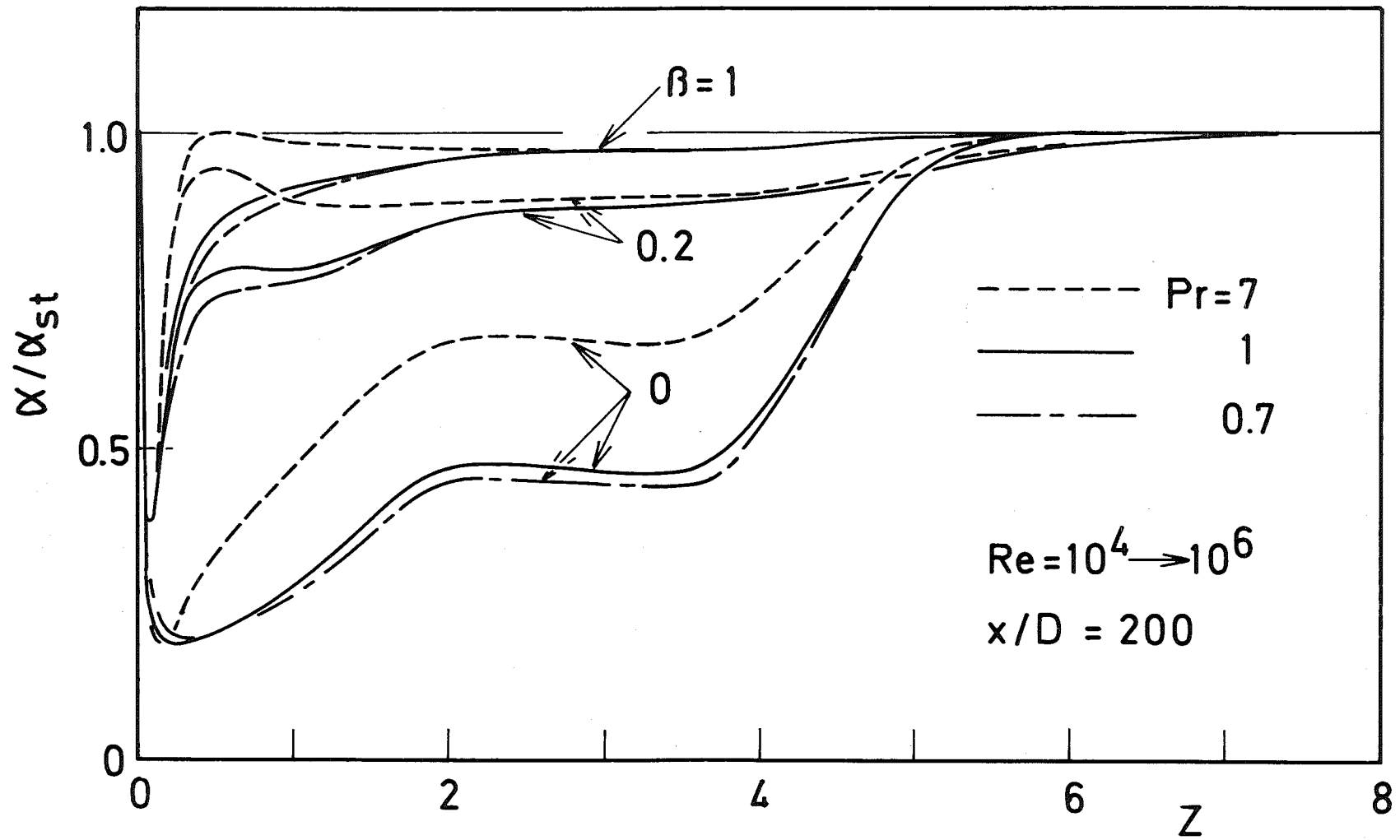


Fig. 18 Effects of  $Pr$  and  $\beta$  on the variation of  $\alpha/\alpha_{st}$  in accelerated flow.

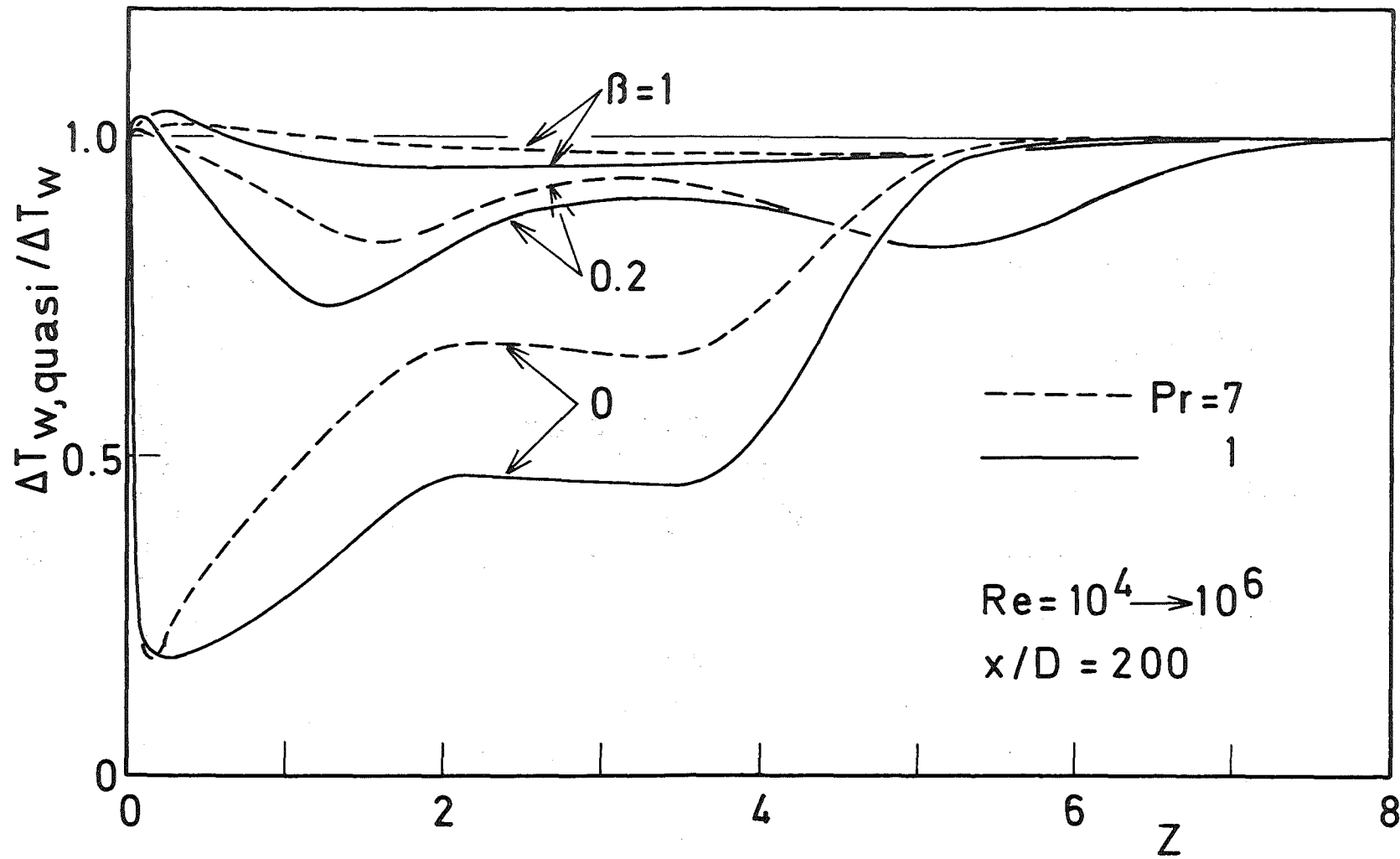


Fig. 19 Variation of  $\Delta T_{w,quasi} / \Delta T_w$  in accelerated flow.

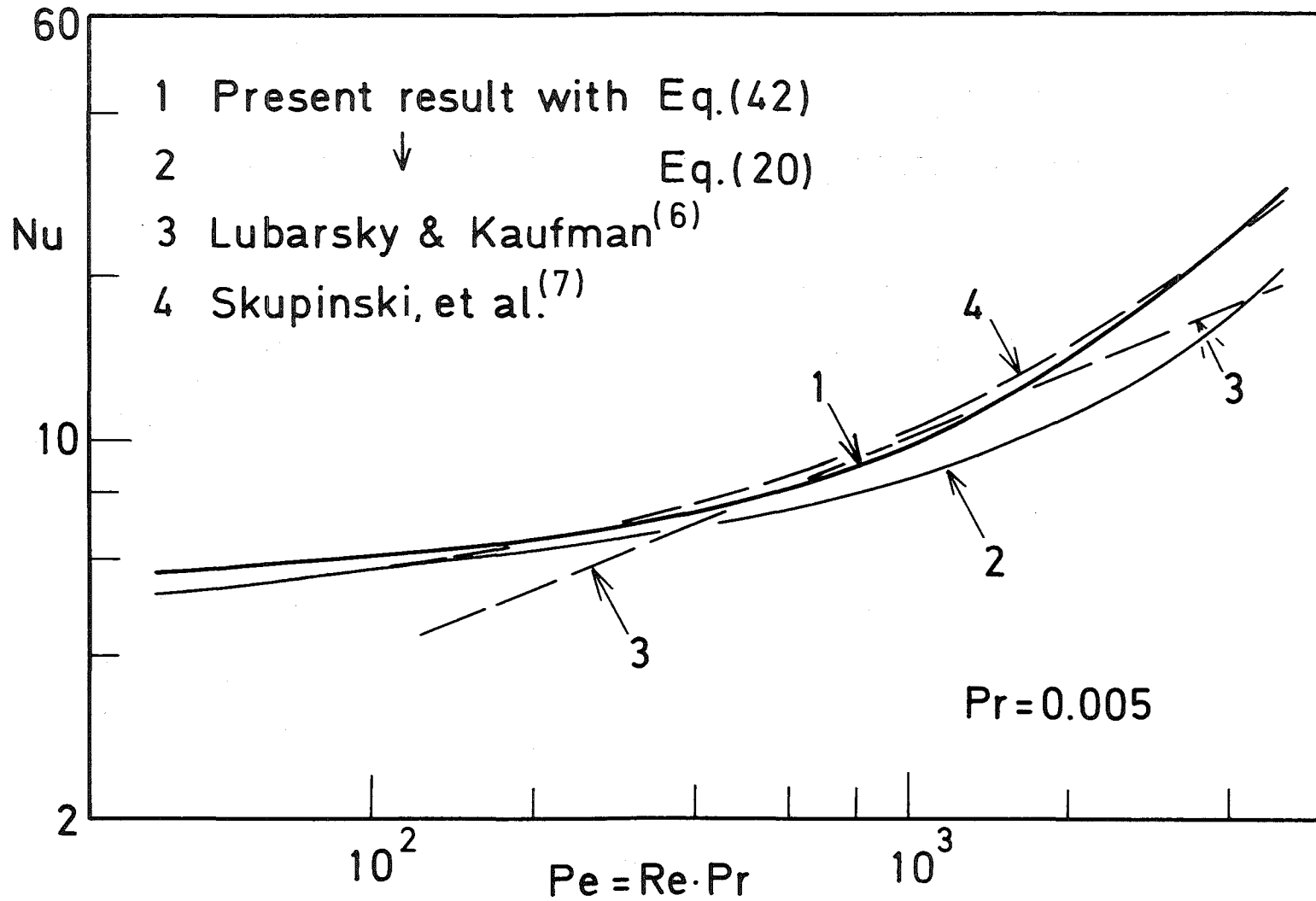


Fig. 20 Steady state heat transfer coefficient for a small Prandtl number.

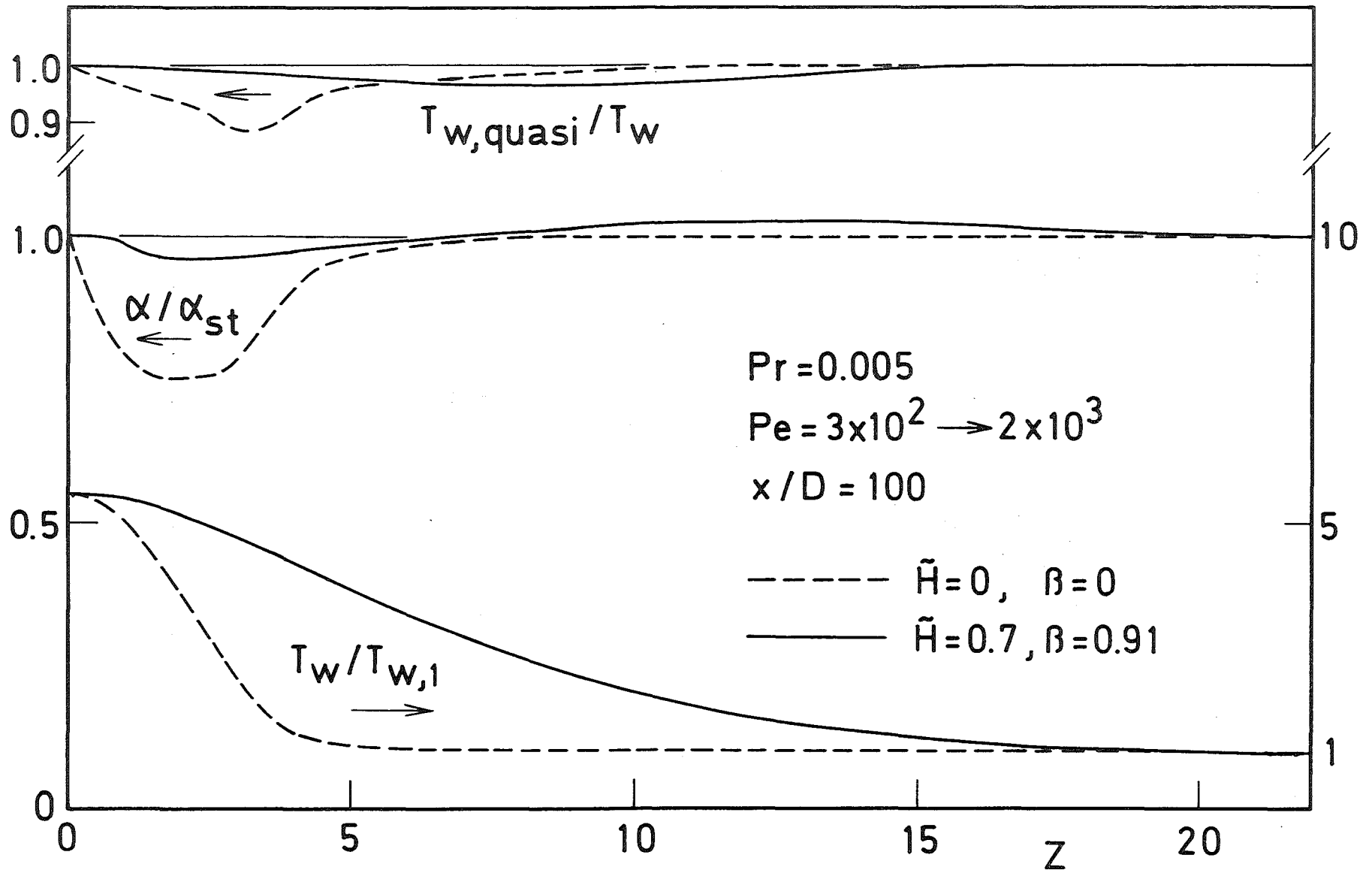


Fig. 21 Transient heat transfer of a liquid metal cooling in accelerated flow.

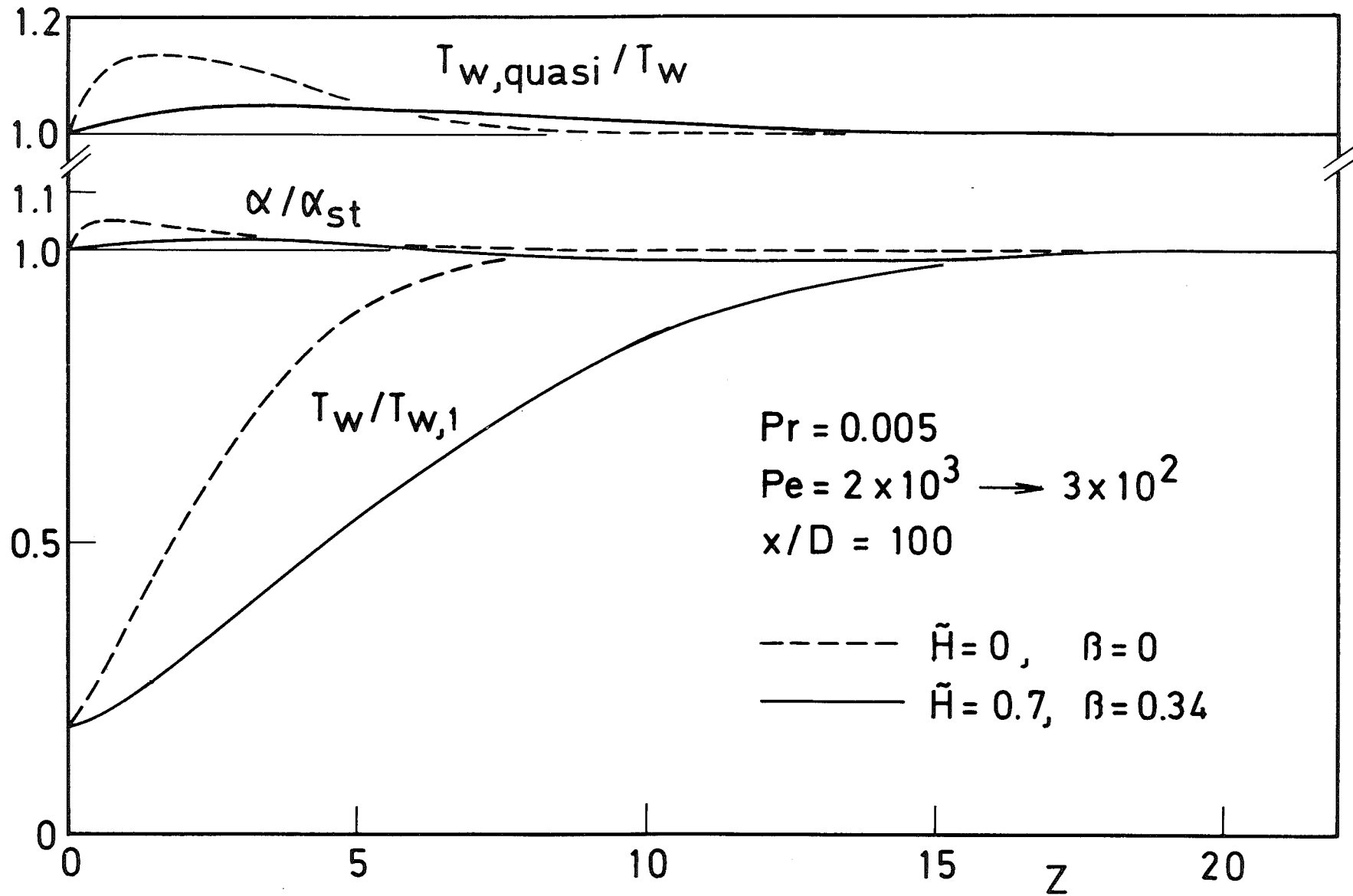


Fig. 22 Transient heat transfer of a liquid metal cooling in decelerated flow.